

Disclaimer/Publisher's Note: The statements, opinions, and data contained in all publications are solely those of the individual author(s) and contributor(s) and not of MDPI and/or the editor(s). MDPI and/or the editor(s) disclaim responsibility for any injury to people or property resulting from any ideas, methods, instructions, or products referred to in the content.

Article

Chemometrics of the Environment: Hydrochemical Characterization of Groundwater in Lioua plain (North Africa) using Time Series and Multivariate Statistical Analysis

Ali Athamena ¹, Aissam Gaagai ², Hani Amir Aouissi ^{2,3,4}, Juris Burlakovs ⁵, Selma Bencedira ^{4,6}, Ivar Zekker ⁷, and Andrey E. Krauklis ^{8,9*}

¹ Department of Geology. Institute of Earth and Universe Sciences. University of Batna 2, 05078 Fesdis, Algeria; a.athamena@univ-batna2.dz

² Scientific and Technical Research Center on Arid Regions (CRSTRA), 07000 Biskra, Algeria; gaagai@univ-batna2.dz

³ Laboratoire de Recherche et d'Etude en Aménagement et Urbanisme (LREAU), USTHB, Algiers 16000, Algeria; aouissi.amir@gmail.com

⁴ Environmental Research Center (CRE), Badji-Mokhtar Annaba University, Annaba, 23000, Algeria.

⁵ The Mineral and Energy Economy Research Institute of the Polish Academy of Sciences, Wybickiego 7, 31-261 Kraków, Poland; juris@geo-it.lv

⁶ Laboratory of LGE, Department of Process Engineering, Faculty of Technology, Badji Mokhtar Annaba University, Annaba 23000, Algeria; selmaben30@yahoo.fr

⁷ Institute of Chemistry, University of Tartu, 14a Ravila St., 50411 Tartu, Estonia; ivar.zekker@gmail.com

⁸ Institute for Mechanics of Materials, University of Latvia, Jelgavas Street 3, LV-1004 Riga, Latvia;

⁹ Department of Environmental Science, Faculty of Geography and Earth Sciences, University of Latvia, Raina Blvd 19, LV-1586 Riga, Latvia;

*Correspondence: Andrey E. Krauklis (A.E.K.); Mail : andrejs.krauklis@lu.lv; andykrauklis@gmail.com

Abstract: Drinking water quality is a major concern, especially in African countries. This manuscript aims to analyze the chemical composition of Lioua's groundwater in order to determine the geological processes influencing the chemical elements' composition and origin. Therefore, chemometrics techniques such as multivariate statistical analysis (MSA) and time series methods (TSM) are used. Indeed, MSA includes a component analysis (PCA) and a cluster analysis (CA), while autocorrelation analysis (AA) supplemented by simple spectral density analysis (SDA) is used for TMS. PCA displays three main factors explaining a total variance (TV) of 85.01 %. Factors 1, 2, and 3 are 68.72%, 11.96%, and 8.89 % of TV, respectively. In the CA, three groups were controlled by TDS and EC. G1 reveals a close association between SO_4^{2-} , K^+ , Ca^{2+} , and TDS; G2 reveals a close association between Na^+ , Cl^- , Mg^{2+} , and EC; G3 shows the dissociation of bicarbonates HCO_3^- and NO_3^- from other chemical elements. AA shows a linear interrelationship of EC, Mg^{2+} , Na^+ , K^+ , Cl^- , and SO_4^{2-} . However, NO_3^- and HCO_3^- indicate uncorrelated characteristics with other parameters. For SDA, the correlograms of Mg^{2+} , Na^+ , K^+ , Cl^- , and SO_4^{2-} have a similar trend with EC. Nonetheless, pH, Ca^{2+} , HCO_3^- and NO_3^- exhibit multiple peaks related to the presence of several distinct cyclic mechanisms. The methods enabled the authors to conclude that the geochemical processes influencing the chemical composition are: (i) dissolution of evaporated mineral deposits, (ii) water-rock interaction, and (iii) evaporation process. In addition, Groundwater exhibits two bipolar characteristics, one recorded with negative and positive charges on pH and Ca^{2+} and another recorded only with negative charges on HCO_3^- and NO_3^- . On the other hand, SO_4^{2-} , K^+ , Ca^{2+} , and TDS are the major predominant elements in the groundwater's chemical composition. The major participation of salts and chlorides is in the electrical conductivity of water. The dominance of the lithological factor in the overall mineralization of the Plio-Quaternary surface aquifer waters. The origins of HCO_3^- and NO_3^- are different. Indeed, carbonated for HCO_3^- has a carbonate origin, whereas NO_3^- has an anthropogenic origin. The salinity was affected by Mg^{2+} , SO_4^{2-} , Cl^- , Na^+ , K^+ , and EC. Ca^{2+} , HCO_3^- and NO_3^- are resulted from human activity fertilizers, the carbonate facies outcrops, and domestic sewage.

Keywords: Chemometrics; Wastewater; Hydrochemical Characterization; North Africa; Environmental Science; Groundwater; Data Analysis; Time Series; Multivariate Analysis; Statistics.

1. Introduction

Water is an essential compound of everyday life, and it is so familiar that we often forget its role, importance, and necessity. Undoubtedly, water is a vital resource for nature and living beings [1,2]. In developing countries with arid climates, groundwater is crucial since it is often the only source of drinking water and is, therefore, vital for developing these countries [3]. The increased dependency on groundwater has made water conservation a top priority in water management studies. Improper operation of groundwater resources would not only cause a shortage of water resources but would also lead to changes in water quality [4].

Groundwater contains a wide variety of dissolved solids in various concentrations due to chemical interactions with geological layers through which it flows and, to a lesser extent, because of other factors like atmospheric, surface water, and anthropogenic activities [5,6]. Groundwater constitutes a memory that brings on the surface indications of the deep reservoir [7]. It is clear that the chemistry of groundwater depends, particularly, on the lithological composition of the layers crossed and on the contact time. Consequently, the elements, which are in the solution, are informative on the nature of the aquifer crossed [8]. Nonetheless, quality, which is a combination of chemical, physical, and biological parameters, is a somewhat subjective term since its real value depends on the specifics of a particular use case [9]. Increasing the knowledge of the geochemical evolution of water in arid and semi-arid regions could improve the understanding of the hydrogeochemical systems in the water table, leading to the sustainable development of water resources and effective water management. Identifying the factors affecting water quality using suitable evaluation methods is necessary. The feasibility study for a given area is fundamental before the establishment of any related applied research works.

Presently, researchers have found increased interest in using linear models and multivariate statistical analysis for sustainable groundwater resource management [10,11]. For a better characterization of the hydro-geochemistry, chemometric methods and saturation indices were used in the literature [12–14]. Chemometrics has long been considered useful in obtaining information from environmental data that could be interpreted to uncover useful correlations [15–18]. Chemometric techniques such as principal component analysis (PCA) and cluster analysis (CA), along with geographical information system (GIS) techniques, aid in the interpretation of the large dataset for a better understanding of the geochemical evolution and sources of the pollution in the alluvial aquifers [17].

Linear modeling should be mentioned, such as the time series, multivariate analysis, and geostatistical techniques [5,19,19–21] applied multivariate analysis to study the chemical changes in groundwater using CA (cluster analysis) and PCA (principal component analysis) [22,23], used factor analysis (FA) to discuss mineralization, geochemical evolution, and finally, groundwater contamination. In addition, according to Roubil et al. [24], CA has been used to interpret the hydrochemical data. Many scientists used this method to study the chemical evolution of water along the groundwater flow [25] as an example. This method enables the verification of spatial and temporal variations caused by anthropogenic and natural factors [26].

Concerning time series analysis, the method is considered one of the most useful techniques applied in modeling and forecasting water quality [27]. At present, time series analyses are used in various sciences such as economy, natural sciences, physics, and engineering. Water resources engineering also belongs to this category since many characteristics of streams, water bodies, and groundwater resources, as well as seas and lakes, are defined using time series [28]. Therefore, it can be useful in modeling and in developing an understanding of the process or a phenomenon, as well as in forecasting future

values based on past observations and data [29,30]. The linear dependency of successive values over a time period is given by autocorrelation analysis, and the autocorrelation function is expressed as variance and auto covariance of time series data [31]. At the same time, the simple spectral density analysis completes the autocorrelation analysis [32].

In Algeria, in recent years, the development of irrigated crops in the South of the Country (Region characterized by an arid climate and located beyond the isohyet of 150 mm/year), while perennial agriculture of date palms or greenhouse crops requires much more water from irrigation, has been based chiefly on groundwater pumping. Such practice ensured higher income for farmers, but it is also responsible for the degradation of water quality (salinization), especially that of the region's groundwater resources. The soils of the Saharan regions of Algeria are rich in soluble salts, which accumulate and often present calcareous or gypseous or calcareous-gypseous crusts. The presence of these gypsum, limestone, and saline accumulations, in general, poses many problems for the physicochemical quality of groundwater via water-soil interaction. This is the case in the Lioua region.

The main aim of the present study is to examine the chemical composition of groundwater while determining the origin of the chemical elements found in the waters using chemometric techniques such as time series and multivariate statistical analysis methods. The techniques mentioned will be used for all the samples taken from a potential underground water resource, massively exploited, located in the arid region of Algeria's Lower Saharan region. This is the surface aquifer of the Plio-Quaternary aquifer, intended for drinking water supply and irrigation of the Lioua region.

This article also elucidates the use of the chemometric technique for the analysis and interpretation of water quality data for the rational management of groundwater resources in arid regions. The results of this study will provide important information on the quality of groundwater in the study area and help adopt an appropriate remedial management approach in other agricultural regions similar to Lioua of the lower Sahara of Algeria.

2. Materials and Methods

2.1 Study area

The province of Biskra is located in the Southeast of Algeria and, more precisely, in the South of the Aurès, constituting its natural limit in the North. It extends to the Southeast to the Chotts area (Chott Melghir) and to the Southwest to the beginning of the great eastern erg. Geo-physically, the wilaya extends over an area of 12755 km² and is made up of large geographical units: to the North, a mountain and high plateau area, to the Southeast, an area of the Chotts to the east and to the South, an area of plateaus and steppe plains on the El Outaya-Doucen axis in the center. The majority of the lands of the wilaya have a large flat expanse followed by a low-pressure area, that of Chott Melghir, Figure 1.

Lioua is a commune of Biskra Province that is located about forty kilometers south of Biskra (Figure 1). Located on Oued Djedi; it extends over an area of approximately 242.1 km² at an altitude of 94 m. It is part of the Zab Gharbi palm groves in the Oued Djedi watershed. The study area belongs to the lower arid bioclimatic level ($200 < P > 100$ mm) with a strong continental influence. Rainfalls are usually falling as heavy downpours. The average temperature throughout the year is 22.4 °C, with a high seasonal variation. The maximum temperature can reach 50 °C during the presence of superheated air from the South.

The region of Lioua has an agricultural vocation par excellence where intercropping market gardening and that of fruit trees are practiced intensively in the oases of date palms. The agricultural area is estimated at 7495 Ha; according to the direction of the agricultural services of the wilaya of Biskra, the region has 1160 boreholes irrigating an area of 4902 Ha and 50 wells irrigating 116 Ha. In arid areas and faced with the virtual absence of surface water resources, the exploitation of groundwater remains the only way to meet needs. Agriculture is a productive sector characterized by the greatest demand for water, mainly due to farming needs higher than rainfall contributions. In addition, the generalization of irrigation is being spread over large agricultural perimeters, where the productive potential of the soil is closely linked to the availability of water during the summer period [8].

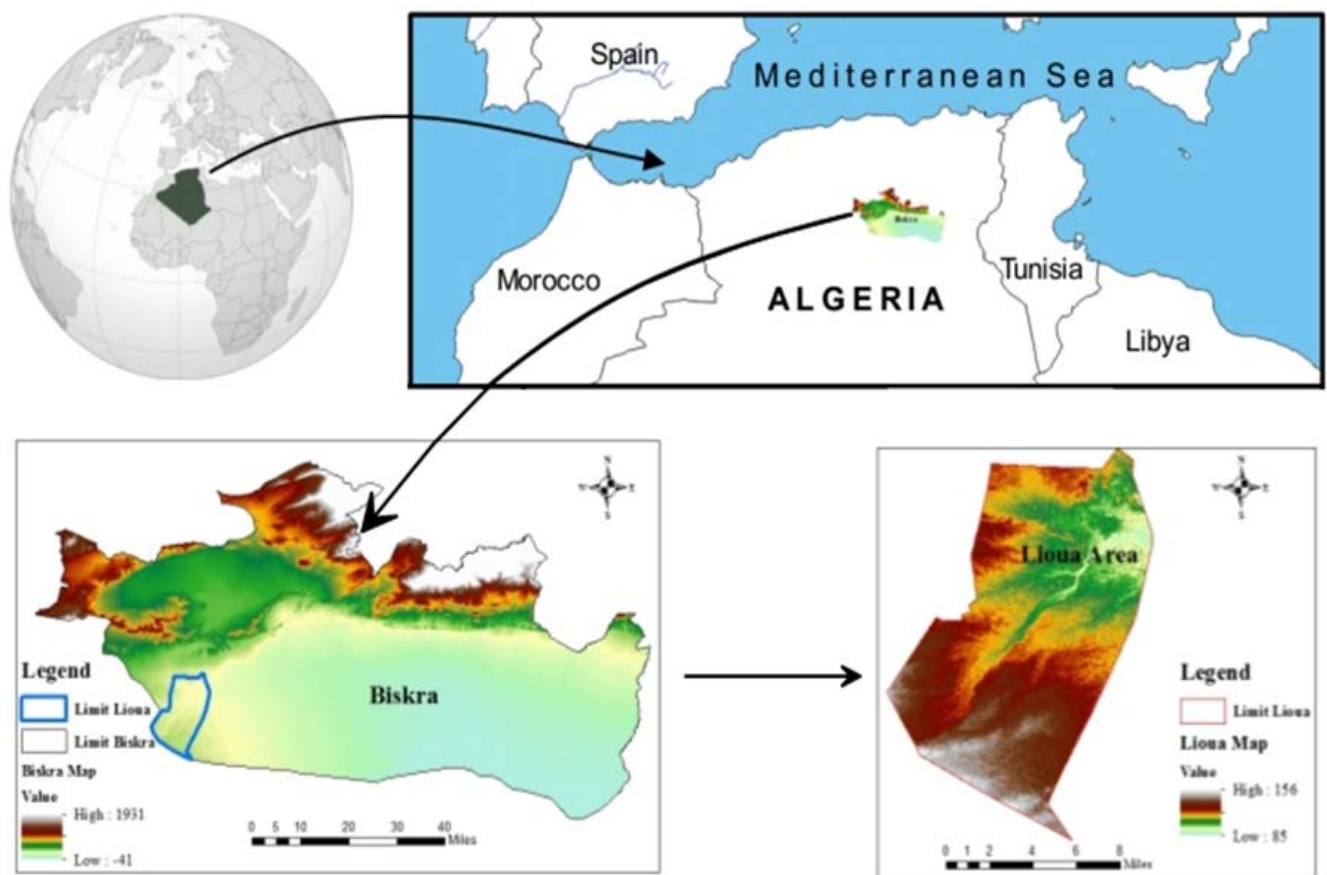


Figure 1. Location map of the study area.

2.2 Geological and hydrogeological setting

The region of Biskra is mainly characterized by sedimentary terrains, ranging from Barremian (Cretaceous) at the base to Quaternary at the top. The lower Sahara is, in fact, a vast backfilling plain, which has slowly subsided since the upper Cretaceous to the Quaternary. This basin is filled with post-Eocene continental Tertiary deposits, made up of agglomerated sands intercalated with clay layers and clay-sand banks [33]. The Neogene deposits, which are mainly the product of the dismantling of the Atlas chain, completely mask the underlying folded structures. In addition, it is only thanks to geophysics and drilling logs that this structure is updated [30].

Litho-stratigraphically, the Lioua region is made up of formations of ages ranging from Secondary to Quaternary. Secondary formations (Cretaceous) consist of limestone,

crystalline limestone, dolomites, sandstone, gypsum, anhydrite, clays, and marls, while Tertiary formations (Paleogene and Neogene) consisting of limestone, marls, gypsum, clays, gravel and sand red. The Quaternary formations consist of scree, pebbles, gravel, sand, gypsum limestone, sandy alluvium, and clay alluvium (Figure 2).

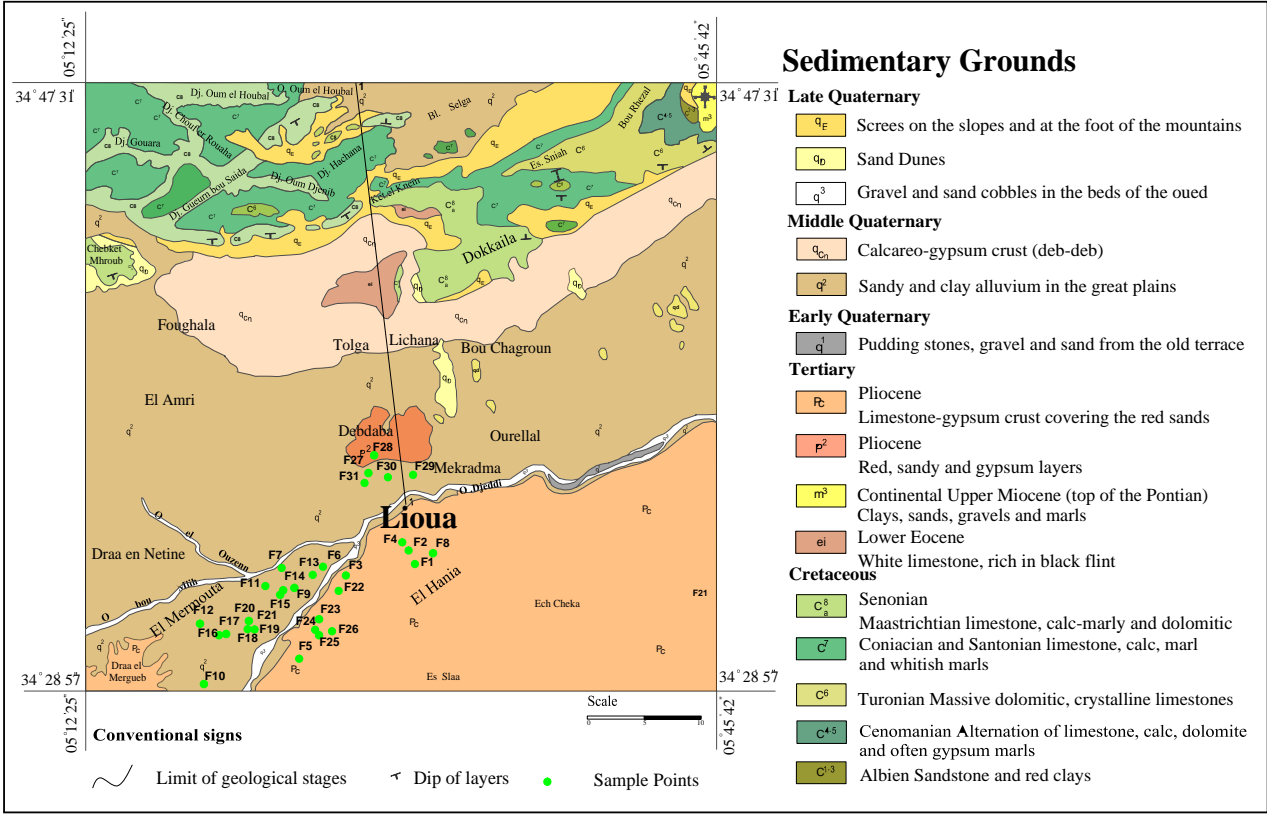


Figure 2. Extract from the Geological map of Biskra, Sheet N°48, Scale 1/200 000, with groundwater sampling points of the research area.

For the hydrogeological context, geological and hydrogeological studies have made it possible to highlight the existence of several aquifer reservoirs of very distinct importance in terms of their lithological constitution, their geological structure, and the ease with which they are exploited. These aquifers belong to the Quaternary, Mio-Pliocene, Lower Eocene and Upper Senonian (Maastrichtian), and Albian. The Albian aquifer also called the continental intercalary (CI) aquifer, is by far the most important reservoir in the region since it covers most of the northern Saharan territory. Thus, groundwater belongs to a complex hydrogeological basin whose main aquifer reservoirs are shown in Figure 3 and 4.

The water table of Oued Djedi particularly represents the superficial water table. The thickness of this water table varies between 50 and 70 m, with an average flow of 20 l/s. The quality of the water extracted is poor to average; only south of Lioua, it is of good quality. The aquifer reservoir is heterogeneous and consists of detrital materials (pebbles, gravel, and sand). The substratum is made up of a thick clay formation; sometimes, it appears in the form of lenses of sand in discordance with the layers of clay. The water table is fed by rainwater, seepage from the Oueds, and irrigation water.

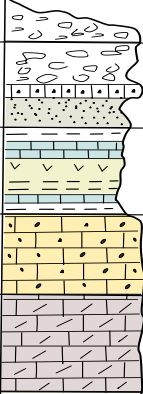
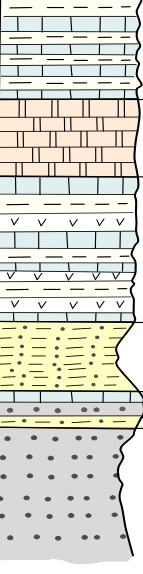
Stratigraphic unit	Stratigraphic Log	Stratigraphic Description	Litho-Stratigraphic Unit	Hydrogeological Unit	
Quaternary		Alluvium	Continental	Water Table	Terminal Complex
Mio-Pliocene		Gypsum Limestone Pudding Sand, Clay	Terminal	Sand Table	
Middle Eocene		Clay, Gypsum Dolomite Limestone	Clay Evaporitic Eocene	Semi-impermeable middle Eocene Aquifer	
Lower Eocene		White Flint Limestone	Carbonate Eocene	Table Water of Limestone	
Upper Senonian		Dolomitic Limestone	Senonian Carbonate		
Lower Senonian		Alternation of Limestone and Marl	Senonian Lagoon	Impermeable	
Turonian		Dolomitic Limestone	Carbonate Turonian	Turonian Limestone Table	
Cenomanian		Marl-Limestone Marls Gypsum	Clay-Evaporitic Cenomanian	Impermeable	
Albian		Clays Sandstone	Albien Argillo Sandstone	Continental Intercalaire Aquifer	
Aptian		Limestone, Clay Marl, Sandstone	Albian Sandstone Lagoon		
Barremian		Sandstone	Barremien Sandstone		

Figure 3. Summary of the geological and hydrogeological units of the Biskra region.

The Mio Pliocene sands table is essentially constituted by an alternation of sands, gravels, and clays. It is strongly exploited by a very important number of drillings intended essentially for the irrigation of agricultural lands. The thickness of this aquifer varies from 80 to 140 m with a flow rate of 5 to 15 l/s. The aquifer is made up of several producer levels with a heterogeneous composition: detrital materials, gravel, and sand wrapped in a clay matrix. At depth, the formation becomes predominantly sandy-clay and rests on an impermeable formation composed of gypsum marl and anhydrite of the middle Eocene. The sands sheet is covered by a shallow alluvial deposit or a Quaternary gypsum sand layer. In places, the Mio-Pliocene outcrops bring this aquifer into direct contact with the surface, thus ensuring its supply from surface water [34].

The Lower Eocene limestone aquifer is the most solicited aquifer in the Ziban region (Zab El-Gharbi). It has been well known for a long time for its artesianism and its natural outlets, which are the North-East springs of the Lioua region (Oumache, M'lili, Megloub). The thickness of this aquifer varies from 150 to 250 m with a flow of 5 to 40 l/s. This aquifer contains important reserves, which are linked to the facies, the state of fissuring of the rock, and to the underground recharge from the Saharan Atlas. Its roof is constituted in

the North by sandy-clay formations of the Mio-Pliocene and in the South by marls with gypsum of the middle Eocene, contributing to its loading [35]. The reservoir of the limestone nappe is essentially made up of limestone of the lower Eocene, upper Senonian, and Turonian.

The continental intercalary aquifer (Albo-Barremian) is a very deep nappe (more than 2000 m), often called Albian. It is characterized by warm waters whose temperature can exceed 60 °C and bad chemical quality of water. The thickness of this water table varies from 250 to 300 m with a flow of more than 25 to 120 l/s, and it is characterized by its artesianism. It is made up of sandstone, limestone, and clay. It is not solicited in the region, except in Ouled Djellal and Sidi Khaled where the Albian or Barremian sandstone formations are found at depths of 1500 to 2500 m (Figure 3).

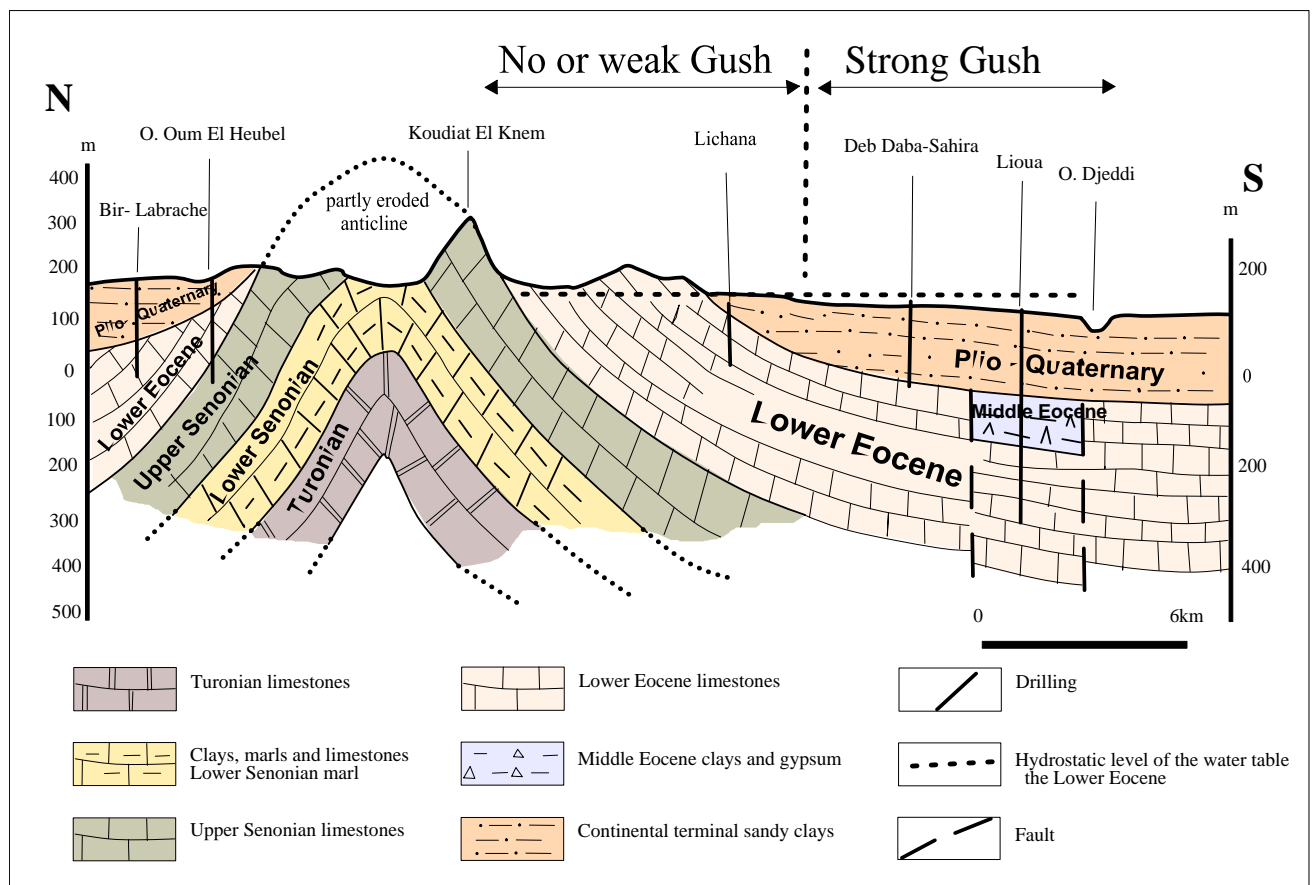


Figure 4. Schematic geological section 1-1 of the study region; established based on the work of G. Mauget updated.

2.3 Groundwater Sampling and Analysis

A total of 31 samples were experimentally taken and analyzed in this study. These included 12 samples collected by the authors in January 2021, and the rest were collected in May 2021. To determine the location sampling points, a global positioning system (GPS) (Model: GPS map 76 CSx) was used, as presented in Figure 2. It is assumed that during/after the rainy season, pollutants may have been subjected to downward leaching, and thus contaminating the underlying aquifers [36]. After pumping for approximately 15 min, the samples were collected after stabilizing the water temperature to remove the groundwater stored in the hydraulic structure; samples were collected using two polypropylene (PP) bottles washed with acid according to the method of the American

Public Health Association (APHA) [37]. Each sample was immediately filtered on-site through 0.45- μm filters of acetate cellulose. Filtrate for cations analyses was transferred into 100 cm³ polyethylene (PE) bottles and immediately acidified to pH < 2 by the addition of ultrapure nitric acid (5 mL 6N HNO₃) (Merck, Germany). Concerning anions analysis samples, they were collected into 250 cm³ polyethylene bottles without acidification. Samples were stored in an ice chest at a temperature of about < 4 °C; then, they were transferred to the laboratory and analyzed.

The physicochemical parameters (electric conductivity, temperature, and pH) were measured using a WTW multiparameter (P3 MultiLine pH/LF-SET). Concerning water samples, they were analyzed for major dissolved chemical constituents. Ca²⁺, Mg²⁺, Cl⁻, and HCO₃⁻ ions were determined by the method of titration. SO₄²⁻ was determined using a spectrophotometric method. Na⁺ and K⁺ were analyzed using a flame photometer. The concentration of TDS was determined by weighing and drying at 103–105 °C in an oven. Nitrates were determined using the cadmium column reduction method. All samples were analyzed in triplicate with analytical uncertainty of less than 4%. To check the correctness of the analysis, the cations–anions balance was used, where it was within $\pm 5\%$, indicating the reliability of the chemical analysis. This was achieved by applying standard methods of the APHA [37]. The respective ionic balance is generally around 5%. Hydrochemical results of all samples were statistically analyzed by using DIAGRAMMES 5.8. The results of the time series analysis and the multivariate statistical techniques were produced by STATISTICA (version 14). Regarding the distribution maps of the major (anion and cation) ions in the studied area, they were performed using GIS (Geographic Information System), specifically with the software ArcGIS (version 10.5.X).

2.4. Methodology

2.4.1 Data Treatment and Multivariate Statistical Analysis

The chemometric analyses, such as PCA and CA, have been highly carried out as unbiased methods for attaining significant information from the hydrochemical dataset in order to understand the sources of major ions and geochemical processes influencing the groundwater quality [17,38,39]. Principal Component Analysis (PCA) techniques are generally used to analyze interrelationships among different sets of groundwater hydrochemical data; this is done to extract the most significant factors and also to reduce the data with minimum loss of information [1]. The chemometric analyses help to simplify and organize large data sets to provide meaningful insight. PCA is a statistical technique for reducing the initial inputs of data variables into a small number of principal components for better interpretation of the data [40,41]. The first principal component (PC1) explains the most variance present in the data set, each subsequent component explaining progressively less variance [42]. Prior to the application of the PCA, a standardization of the chemical parameters is carried out (scale z). This standardization renders each of the parameters dimensionless in order to eliminate potential biases towards a particular parameter of the different unit at high concentrations [43,44]. The varimax rotation method was used to extract the principal components (PCs), considering eigenvalues > 1 as significant for interpretation [45]. In this research, the PCA method was applied to hydrochemical data obtained from the Lioua plain to attain significant information in order to understand the geochemical processes influencing the chemical composition of the groundwater and quality in the studied area.

Cluster analysis (hierarchical clustering) is a useful method of objectively organizing a large data set into groups on the basis of a given set of characteristics. CA comprises a

series of multivariate methods used to find true data groups [46]. The primary objective of CA is to identify relatively homogenous groups or clusters of objects based on their similarities/dissimilarities [47]. The grouping of similar objects occurs first, and eventually, as the similarity decreases, all subgroups are merged into a single cluster. This can ultimately assist in recognition of potentially meaningful patterns [48]. In clustering, it is known that the objects are grouped such that similar objects fall into the same class [49]. Cluster analysis (CA) is performed on the standardized data set by means of Ward's method using Euclidean distance as a measure of similarity to obtain a Dendrogram.

Therefore, Ward's method as a linkage rule for classifying the hydrogeochemical data is applied in the present study. The Euclidean distance was used as a measure of distance between samples, which is one of the most commonly adopted measures [50].

2.4.2. Time series analysis

The main application of a time series analysis applied to environmental systems is to understand seasonal changes and/or trends over time. However, another goal that is often of primary importance is to understand and model the correlational structure in the time series. This type of analysis is generally done on stationary processes. A stationary process is a process that stays constant at any given time point. That is, a stationary time series is one without any systematic change in its mean and variance and does not have periodic variations [51].

A short overview of the mathematical expressions of autocorrelation and spectral density is presented. The theory of correlation was highlighted in detail by [52] and [53]. According to [54], a simple autocorrelation analysis provides quantitative information for linearly dependent successive values in time. Autocorrelation function $r(K)$ is expressed using autocovariance $C(K)$ and variance $C(0)$ of the time series, such as in (Eq. 1):

$$r(k) = \frac{C(k)}{C(0)} \quad c(K) = \frac{1}{n} \sum_{t=1}^{n-k} (x_t - \bar{X})(x_{t+k} - \bar{X}) \quad (1)$$

Where k is a time lag ($k = 0 - m$), n is the number of events, x_t is a single event, \bar{X} is the mean of events, and m is the cutting point. The cutting point is usually determined based on the interval of the analysis and the given circumstance. In cases when time series are strongly interdependent, also involving a long-memory effect, the autocorrelation function indicates a slowly decreasing slope along with the non-zero values over a long-time lag. However, if uncorrelated, e.g., rainfall, the autocorrelation function decreases quickly and reaches a zero value in a very short time [55]. A simple spectral density analysis complements the autocorrelation analysis. The spectral density function signifies a transition from a time mode to a frequency mode by applying a Fourier transformation to the autocorrelation function [56]. The spectral density function, $S(f)$, can be interpreted by identifying the different peaks, which stand for periodical phenomena. $S(f)$ characterizes the system as in (Eq. 2):

$$S(f) = 2[1 + 2 \sum_{k=1}^m D(k)r(k) \cos(2\pi f k)] D(k) = \frac{(1 + \cos \frac{2\pi k}{m})}{2} \quad (2)$$

Where f is the frequency, and $D(k)$ ensures that estimated values $S(f)$ are not biased.

3. Results

Thirty-one groundwater samples from a highly agricultural plain in the Lower Sahara of Algeria were experimentally obtained and analyzed. A descriptive statistical summary of the analyzed groundwater samples' parameters, along with the drinking water standards of the World Health Organization [57], is provided in Table 1. The spatial distribution map of major ions (Ca^{2+} , Mg^{2+} , Na^{+} , K^{+} , HCO_3^{-} , SO_4^{2-} , Cl^{-} , NO_3^{-}) of the groundwater samples in the study region are summarized and discussed herein (Figure 5 and 6).

Table 1. Descriptive analysis results of the groundwater samples in the study area.

Parameters	Min	Mean	Max	St Dev	Coef. of variation (CV, %)	WHO (2017) Second Addendum 2021
Ca^{2+}	252	452.71	640	117.89	0.26	150
Mg^{2+}	52.8	172.61	439.2	84.66	0.49	70
Na^{+}	47.73	373.16	1358.54	260.41	0.7	200
K^{+}	5.01	12.02	25.63	4.66	0.39	12
HCO_3^{-}	129.32	187.6	283.04	43.32	0.23	500
SO_4^{2-}	571.43	1636.22	3028.57	647.01	0.4	250
Cl^{-}	106.5	462.07	1462.6	277.65	0.6	250
NO_3^{-}	0.2	37.13	153.44	30.31	0.82	50
pH	7.03	7.64	8.16	0.3	0.04	6.5- 8.5
EC	2000	4370.97	10000	1617.88	0.37	1500
TDS	1232.00	3333.45	7145.00	1269.12	0.38	1000

Remark: units in mg/L except for pH (unitless) and EC ($\mu\text{S}/\text{cm}$); St Dev for standard deviation.

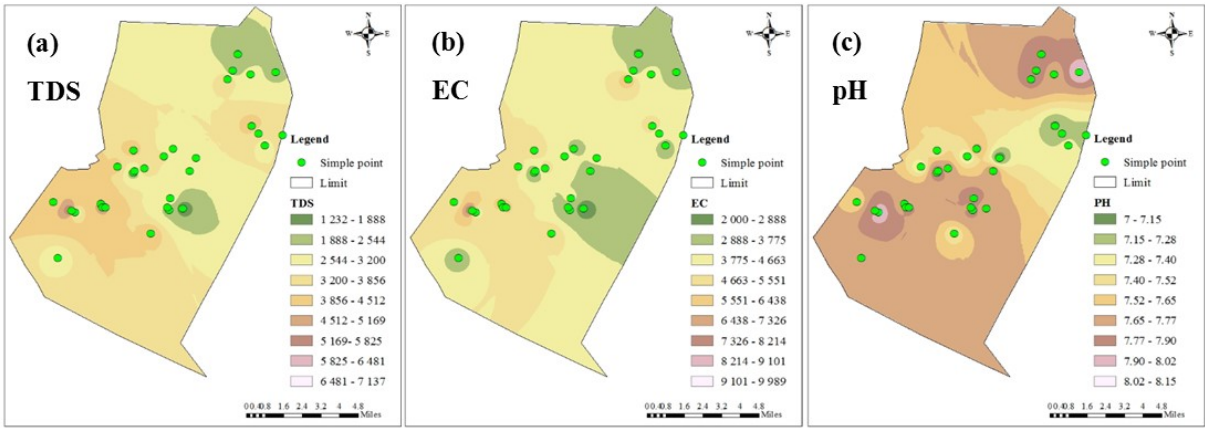


Figure 5. The spatial variation map of the Lioua plain: TDS, pH, and EC.

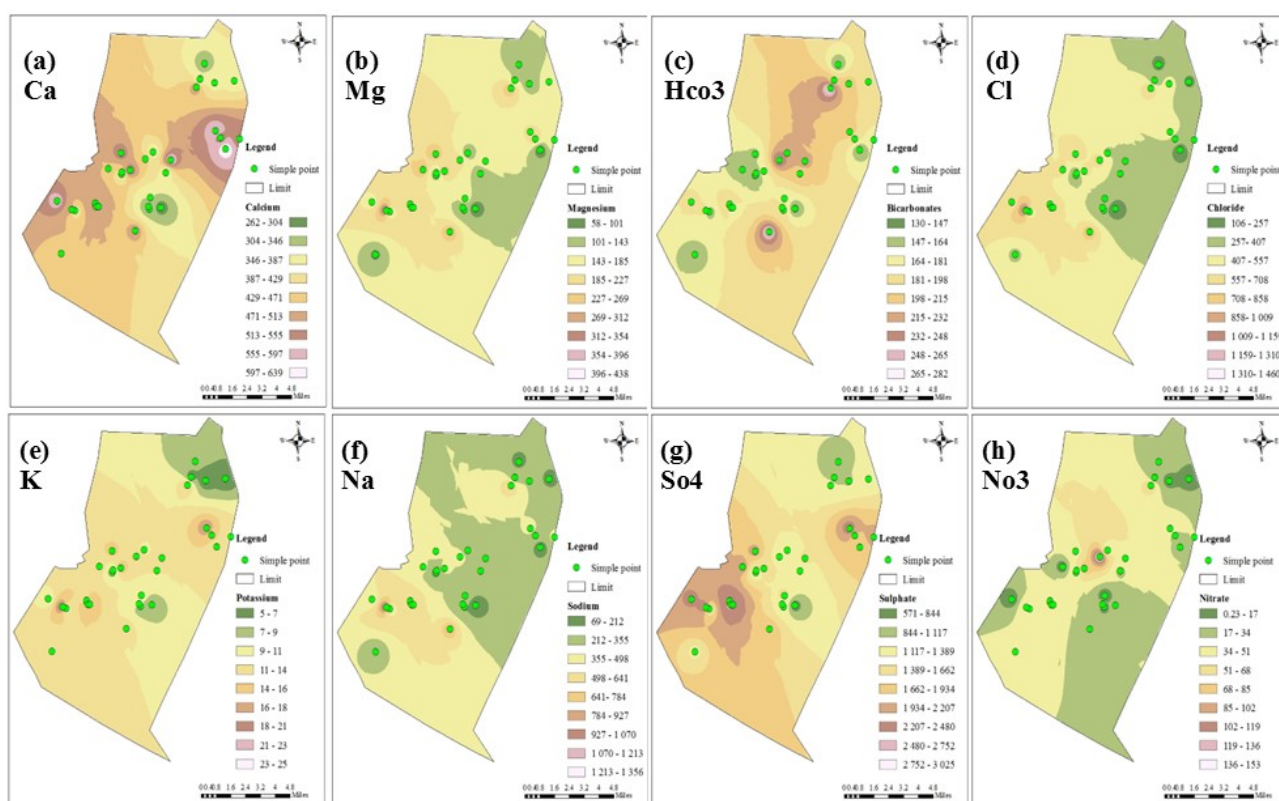


Figure 6. The spatial distribution map of the Lioua plain: major ion concentrations.

3.1. Hydrochemical Water Types and Groundwater Natural Evolution Mechanisms

Groundwater chemistry may reflect the influence of hydrochemical processes occurring in the aquifer [75]. The hydrochemical groundwater types are controlled by major ions, for which the Piper diagram [76] was used in this study. The plotting position indicates a relative composition of groundwater in terms of the cation-anion pairs [77]. The diamond-shaped field of the Piper diagram shows the existence of one major water type: Ca-Mg-SO₄.

For a better understanding of the hydrochemistry and for comparing the water types, Chadha's diagram [80] was plotted (Figure 8). In the present study, all the samples are plotted in the 6th field, representing Ca²⁺-Mg²⁺-SO₄²⁻ type, where Alkaline earths exceed alkali metals and strong acidic anions exceed weak acidic anions.

To study the main mechanisms governing water evolution and the different hydrogeochemical processes controlling groundwater chemistry in the study area, Gibbs plots [81] were applied. The Gibbs plots, (Figure 9) indicates that all of the groundwater samples studied fall in the upper part of the diagrams indicating that evaporation is a major factor in the evolution of groundwater chemistry.

Another approach to reveal the origin and the relationship between the major elements such as: [Ca²⁺ + Mg²⁺] versus [SO₄²⁻ + HCO₃⁻] (Figure 10a), [Ca²⁺/SO₄²⁻] versus [Mg²⁺/SO₄²⁻] (Figure 10b), [Ca²⁺ + Mg²⁺ - HCO₃⁻ - SO₄²⁻] versus [Na⁺ - Cl⁻] (Figure 10c), [Mg²⁺/Ca²⁺] versus [Mg²⁺/Na⁺] (Figure 10e), [Mg²⁺/Na⁺] versus [Ca²⁺/Na⁺] and [HCO₃⁻/Na⁺] versus [Ca²⁺/Na⁺] (Figure 10f) [84]. In order to recognize the ion exchange process between groundwater and aquifer minerals, both chloroalkaline indices was applied (CAI-I and CAI-II) (Eq. 3 and 4; Figure 10d).

$$CAI - I = \frac{Cl^{-}-(Na^{+}+K^{+})}{Cl^{-}} \tag{3}$$

$$CAI - II = \frac{Cl^{-}-(Na^{+}+K^{+})}{SO_4^{2-}+HCO_3^{-}+CO_3^{2-}+NO_3^{-}} \tag{4}$$

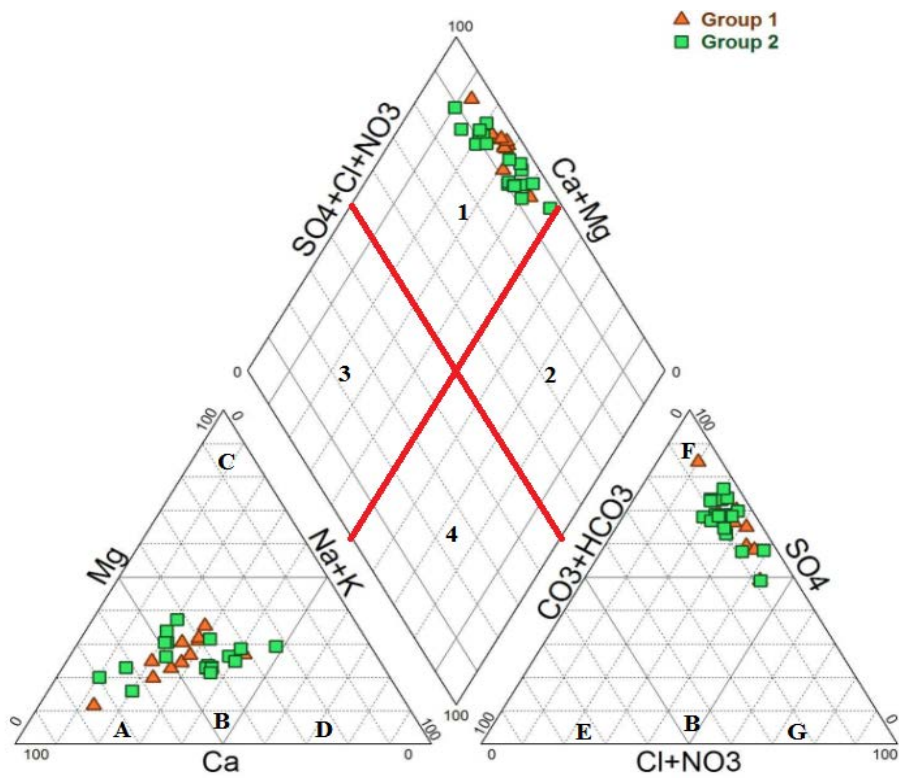


Figure 7. Piper diagram of groundwater samples

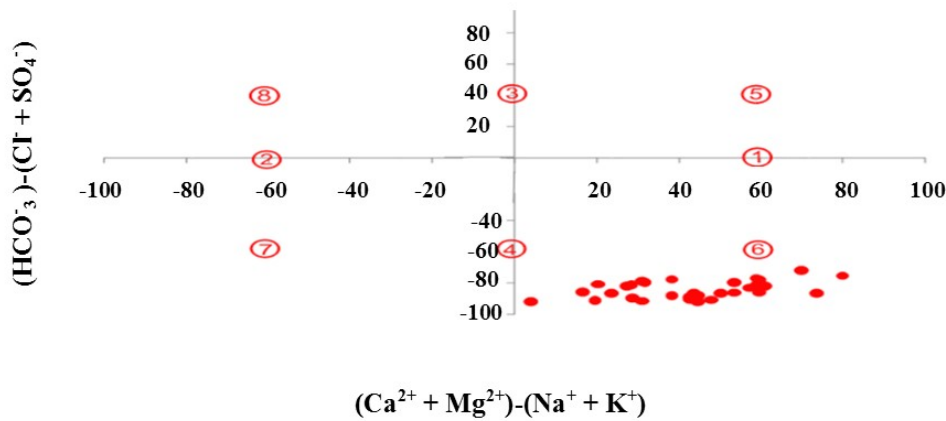


Figure 8. Chadha diagram of groundwater samples

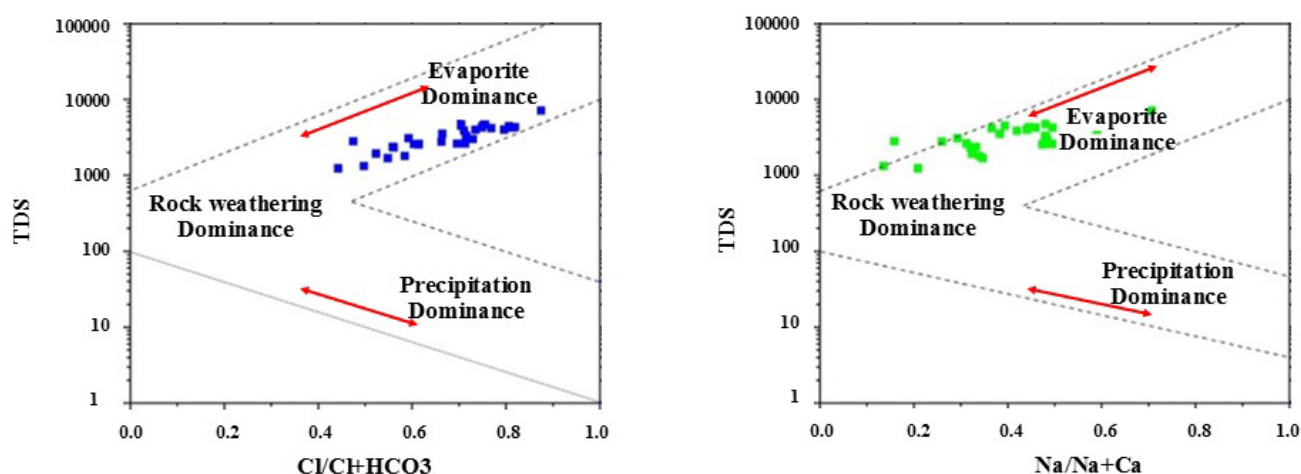


Figure 9. Gibbs diagram of groundwater samples

3.2. Statistical Analysis

3.2.1. Correlation Analysis and Elementary statistics

Furthermore, the acquisition of salinity mechanism has been studied mainly using the correlations of different chemical elements with TDS and EC. Applying Pearson's correlation matrix for the physicochemical data of the samples revealed a moderate to high correlation value (0.62–0.96) between EC, Ca^{2+} , Mg^{2+} , Cl^- , Na^+ , K^+ , and SO_4^{2-} (Table 2). This indicates that these elements are the main components of salinity.

Cv (Coefficient of variation) is usually used to characterize the stability of the variable, which represents the ratio of the standard deviation (SD) to the mean. When the $0 < \text{Cv} < 10$ percent for weak variation; $10\% < \text{Cv} < 100\%$ for moderate variability; $\text{Cv} > 100\%$ strong variation [91]. In this study, the statistical analysis results of 31 groundwater samples from the study area are presented in Table 1.

3.2.2. Principal Component Analysis (PCA)

The analytical results of PCA were performed for the 31 samples and 10 variables. The analysis was carried out on 3 factors, and more than 89.6 % of the total variance having been expressed, the parameter weights for the three components from the PCA of the dataset are given in Table 3 and Figure 11. The percentage of variance, expressed by the first factor (68.72%), shows that there is a fairly good structure in the sampling carried out. This proves that many factors that affect the structure of the samples are linked to each other. This was reflected in the correlation matrix (Table 2), where there was a significant correlation between Na^+ , Cl^- , Mg^{2+} , K^+ , SO_4^{2-} , Ca^{2+} , and conductivity/TDS. These correlations highlight the origin of the salinity of the water of the Plio-Quaternary aquifer of Lioua.

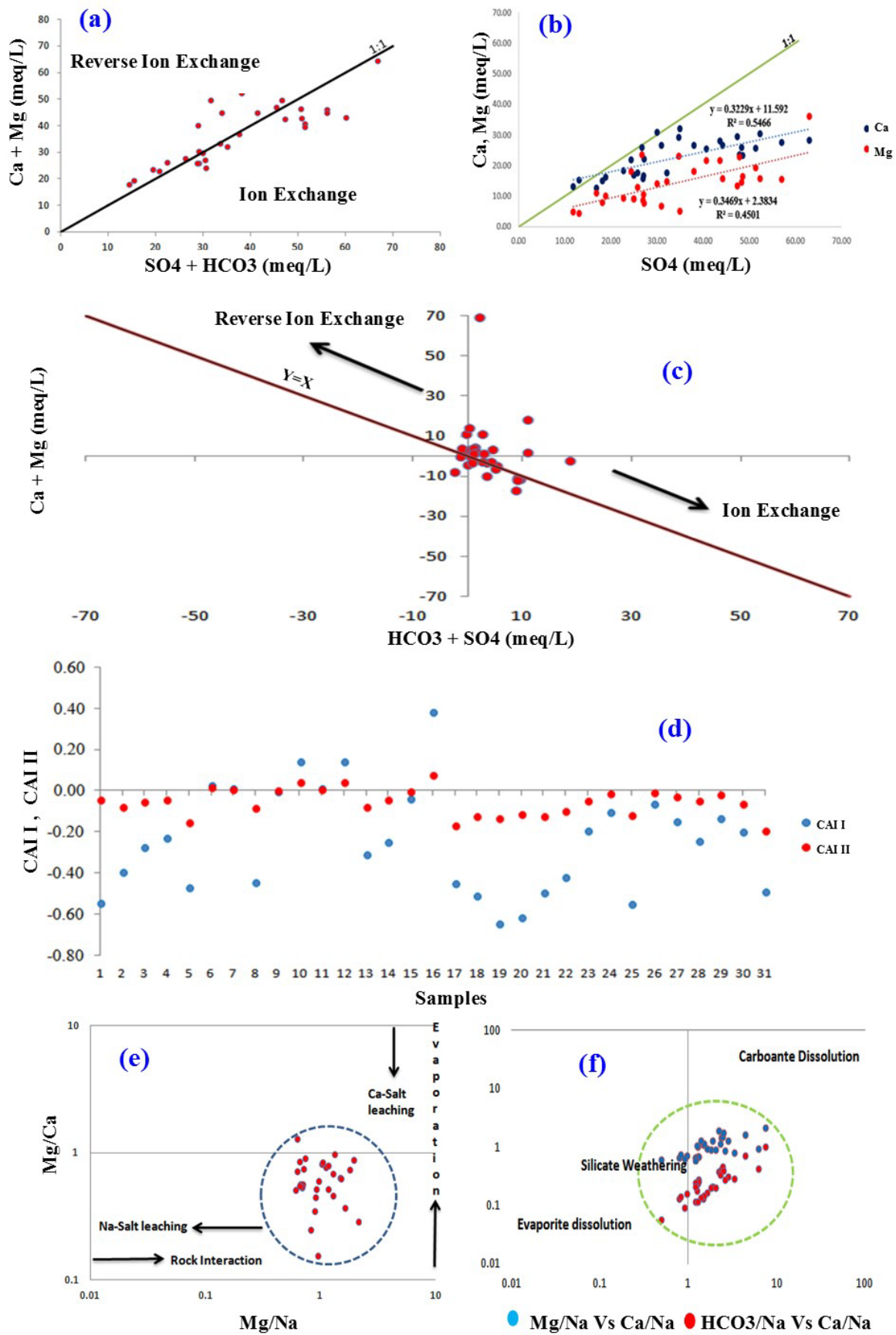


Figure 10. Stoichiometric relations of the major cations and anions of the study water.

Table 2. Matrix of correlation of variables.

Variable	Ca ²⁺	Mg ²⁺	Na ⁺	K ⁺	HCO ₃ ⁻	SO ₄ ⁻	Cl ⁻	NO ₃ ⁻	EC	TDS	pH
Ca ²⁺	1.00										
Mg ²⁺	0.51	1.00									
Na ⁺	0.46	0.88	1.00								
K ⁺	0.66	0.78	0.79	1.00							
HCO ₃ ⁻	0.20	0.43	0.50	0.32	1.00						
SO ₄ ⁻	0.74	0.67	0.70	0.74	0.14	1.00					
Cl ⁻	0.51	0.92	0.95	0.79	0.47	0.69	1.00				
NO ₃ ⁻	0.31	0.32	0.29	0.50	0.33	0.06	0.35	1.00			
EC	0.62	0.92	0.96	0.84	0.44	0.79	0.96	0.33	1.00		
TDS	0.73	0.86	0.90	0.85	0.37	0.93	0.90	0.25	0.96	1.00	
pH	-0.57	-0.25	-0.09	-0.38	-0.27	-0.33	-0.17	-0.21	-0.20	-0.31	1.00

Entries in Bold and italic: significant correlation

Table 3. Factor-variable correlations (factor loadings), based on correlation analysis

Variable	Factor 1 (68.72%)	Factor 2 (11.96%)	Factor 3 (8.89%)
Ca ²⁺	-0.700758	0.259847	-0.487580
Mg ²⁺	-0.914001	-0.058055	0.172156
Na ⁺	-0.933289	-0.073713	0.260453
K ⁺	-0.898108	-0.018727	-0.239490
HCO ₃ ⁻	-0.473047	-0.642695	0.301438
SO ₄ ⁻	-0.828543	0.476478	-0.074104
Cl ⁻	-0.941913	-0.081694	0.191078
NO ₃ ⁻	-0.396510	-0.660032	-0.591586
EC	-0.981341	0.017212	0.113416
TDS	-0.974924	0.192421	0.018904

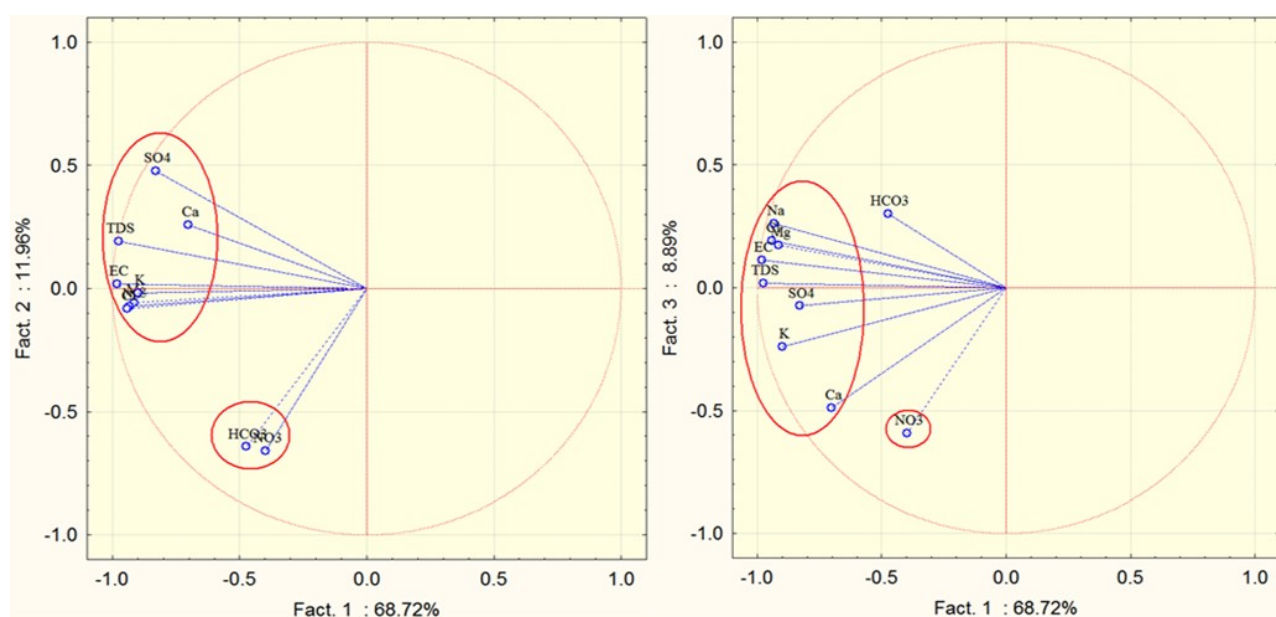


Figure 11. Plots of PCA scores for F2 vs. F1 (left) and F3 vs. F1 (right).

3.2.3. Cluster Analysis (CA)

According to [98], two different methods can be applied to identify clusters, including R- or Q-modes. R-mode is usually applied to water quality variables to reveal the interactions between them (Figure 12). Ward's method as a linkage rule for the classification of the hydrogeochemical data is applied in the present study. The Euclidean distance was used as a measure of distance between samples, which is one of the most commonly adopted measures [50].

In order to compute the similarity of the groundwater samples, a combination of Ward's linkage technique and Euclidean distance was used to execute HCA. A dendrogram of spatial HCA was generated and is shown in Figure 12. For statistical purposes, all of the variables were log-transformed and closely corresponded to normally distributed data. Subsequently, the variables were standardized to their standard scores (z-scores) as described by [99]. Given the fact that there is no particular test to determine the optimum number of groups in the dataset, the visual inspection is the only criterion for the groups' selection in the Dendrogram.

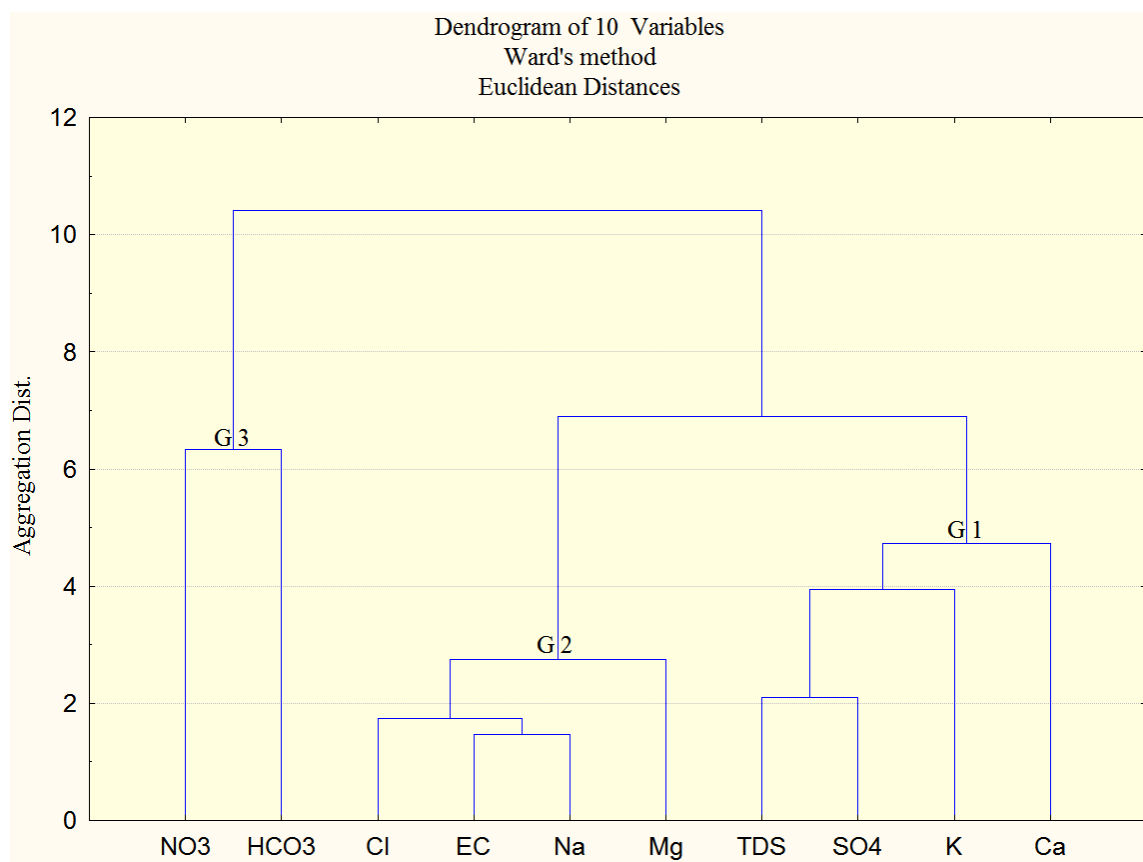


Figure 12. Cluster dendrogram for variables.

3.2.4. Time Series analysis

3.2.4.1. Autocorrelation

The autocorrelation functions of selected hydrochemical parameters such as pH, Ca^{2+} , Mg^{2+} , HCO_3^- , SO_4^{2-} , Cl^- , Na^+ , K^+ , NO_3^- and EC are shown in Figure 13. To study the autocorrelation effect among the 10 variables, the experimental variograms for each of the variables as well as the auto variogram were computed. In total, variogram functions were estimated (Figure 13).

3.3.4.2 Spectral Density

Spectral density functions of all the hydrochemical variables are shown in Figure 14. The behaviors of these functions are similar, and their highest peaks have a single or two points. The correlograms of Mg^{2+} , Na^+ , K^+ , Cl^- , and SO_4^{2-} have an almost similar trend with EC.

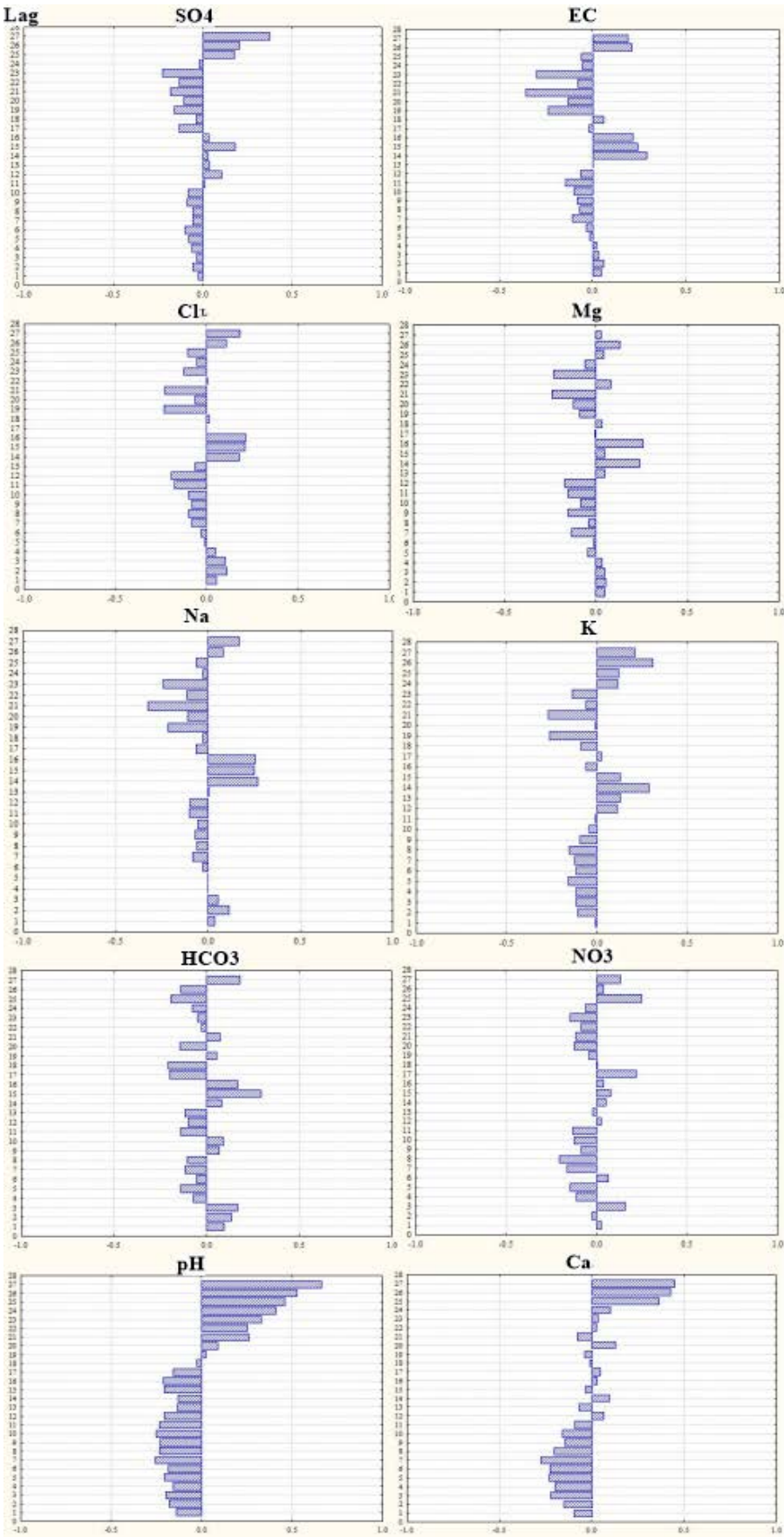


Figure 13. Auto-correlation Function Physicochemical Parameters Time Series.

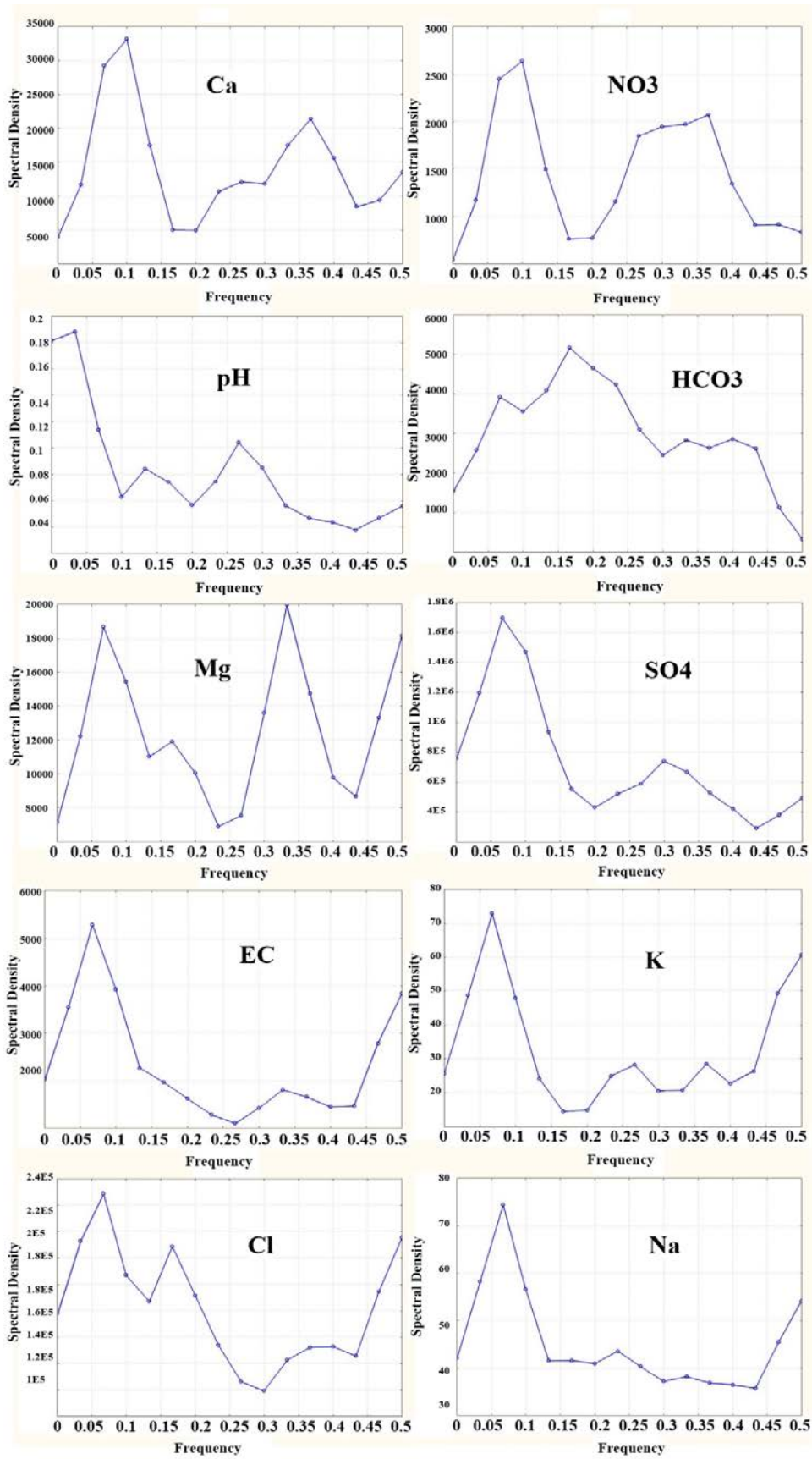


Figure 14. Spectral Density Patterns of Hydrochemical Components in the Study Area.

4. Discussion

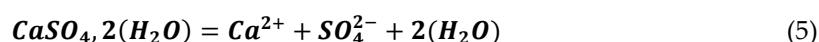
Obtained results show that the mean temperature of the water was 22.7°C with min 11.4°C and max 49.2 °C. The pH value in the study area ranges from 7.03 at F-03 to 8.16 at F-28 with a mean value of 7.64, indicating a weakly alkaline environment, Figure 5c. These values were found to be within the drinking water standards prescribed by the World Health Organization (WHO) [57], ranging from 6.5 to 8.5 (Table 1). The presence of calcium carbonate and magnesium carbonate contributes carbonate ions to the buffering system. Alkalinity is commonly related to hardness, as the main alkalinity source often comes from carbonate rocks (limestone), made up mostly of CaCO_3 [58,59]. It is known that the process of buffering calcite is dominant in the pH range of 6.5–7.5 [60].

The estimation of total dissolved solids (TDS) is essential for understanding the relationship between the environment and groundwater chemistry [61]. The suitability of groundwater with a TDS value above 3000 mg/L is often considered poor, while a TDS level above about 1000 mg/L exceeds the guideline value for human consumption, according to [57]. The maximum TDS was recorded at F-17 with 7145 mg/L, and the lowest value was 1232 mg/L at F-26 with an average value of 3333.45 mg/L in all water samples underground (Table 1). According to the classification of [62], the samples from the study area were classified as unsuitable for consumption and irrigation. The TDS spatial variation map (Figure 5a) shows that the TDS values increased in the Southwestern and northeastern limits, which could be due to the geological characteristics and anthropogenic factors of the study area. The increase in the TDS coincides with the course of the Oueds of the study region Oued Bou-Mlih and Oued El-Ouzenn in the South-West and Oued Djedi, which crosses the plain from the South-West to the Northeast. This configuration leads us to think that the runoff water towards the low points (Oueds) leads to their enrichment in dissolved salts by leaching of the saline soils before their infiltration in the basement via the Quaternary matrix. Likewise, it is known that excessive irrigation leads to increased water salinity, especially since the region is known for its intense agricultural activity.

Electrical conductivity (EC) is the measure of water's ability to carry electrical current; it makes it possible to evaluate the total mineralization of the water. EC shows extremely variable values ranging from 10000 $\mu\text{S}/\text{cm}$ measured at point F-30 in the Southwest to 2000 $\mu\text{S}/\text{cm}$ measured at point F-1 in the Southeast, with an average value of 4370.97 $\mu\text{S}/\text{cm}$ and a coefficient of variation (CV) of 37% (Table 1). However, all the samples' values have been found to be above the guideline value for human consumption as restricted to 1500 $\mu\text{S}/\text{cm}$ according to [57]. Spatial variation of EC, the higher values have been observed in the southwestern and a small area in the northeastern of the study region (Figure 5b). This significant variation in electrical conductivity from one point to another shows heterogeneity in the distribution of the mineral load in the groundwater of the surface aquifer of the Plio-Quaternary of the Lioua region, Figure 5b. This suggests the predominance of the phenomenon of dissolution of salt minerals, and the transport of agricultural inputs by leaching of the land, which consequently leads to an increase in the mineral load in these waters. In the study area, soil salinization is serious and thus requires considerable attention.

Calcium is the preferred element of carbonate rocks. The common source of calcium in the groundwater is limestone in the sedimentary rocks by the dissolution of precipitates of CaCO_3 during the groundwater recharge [63,64]. The concentration of this element in groundwater is mainly controlled by the solubility of certain minerals such as carbonate minerals (calcite and dolomite), gypsum, or silicates [65]. Calcium ion concentration in the groundwater samples varied from 252 to 640 mg/L, with an average concentration of 452.71 mg/L (Table 1). The calcium values in all samples have been above the guide value of 150 mg/L for drinking water, which was prescribed by [57]. The spatial variation map

of Ca^{2+} (Figure 6a) indicates that the highest contents were located in the west and the east center of the study area. These concentrations indicate that these waters are influenced by the dissolution of gypsum formations (Eq. 5).



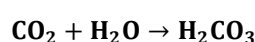
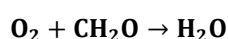
Magnesium comes from the dissolution of carbonate and salt formations. The major source of magnesium (Mg) in the groundwater is due to the ion exchange of ferromagnesian minerals in rocks and the dissolution of dolomite and soils by water [66,67]. In the case of magnesium, the Mg^{2+} ions in water samples ranged from 52.8 to 439.2 mg/L (Figure 6b), with an average value of 172.61 mg/L in all groundwater samples of the study area (Table 1). The highest concentration was found in the F-11 (439.2 mg/L). The guide value of magnesium concentration for human consumption is 70 mg/L [57]. As per the spatial map of magnesium, 42% form the samples in this study area that fall under the guide value are given [57] for drinking water (Figure 6b). The waters of the Lioua plain are rich in magnesium, which leads us to think of an enrichment following the dissolution of evaporites and salt formations such as clays which rich in Mg^{2+} during the recharge of the water table and the leaching of rich soils in magnesium minerals (Debdaba region).

Sodium is found in evaporites (halite NaCl , mirabilite $\text{Na}_2\text{SO}_4 \cdot 10(\text{H}_2\text{O})$). The presence of sodium is linked to the rapid dissolution of evaporitic formations rich in halite. The weathering of rock-forming minerals and agricultural activities may be the main sources of Na in groundwater [67]. Na^+ concentration is in the range of 47.73 to 1358.54 mg/L, with an average of 373.16 mg/L. Only 29% of the samples have Na concentration less than the value guide of drinking water quality of 200 mg/L (Table 1). As the spatial distribution map of sodium (Figure 6f), the highest Na concentration was located in the Northeast (Debdaba region) parts of the study area, exactly in the F-30. These concentrations testify to a salt supply from the evaporites. Nevertheless, it is probable that during their journey, the groundwater may undergo mineralization in contact with the clays constituting the matrix of the Plio-Quaternary aquifers of the region par the phenomenon of base exchange by fixing a Ca^{2+} ion after the release of two Na^+ ions.

In general, potassium rarely exceeds 10 or 15 mg/l in natural waters. The highest contents of potassium are probably induced by weathering of potash feldspars minerals [68]. The minimum and maximum concentrations of potassium in the groundwater samples of the study area varied from 5.01 to 25.63 mg/L, with an average of 12.02 mg/L (Table 1). Accordingly, [57] suggests the value guide of K in drinking water as 12 mg/L. Since the spatial distribution map of K (Figure 6e) revealed that 45% of samples in the study region fall below the value guide of [57] (Figure 6e). These potassium levels come from the alteration of potassic clays and the dissolution of chemical fertilizers (NPK), which are used massively by farmers in the region.

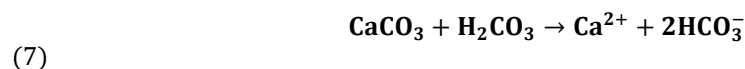
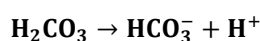
The presence of HCO_3^- and CO_3^{2-} ions are mostly responsible for the alkalinity of groundwater. A major source of HCO_3^- ion in the groundwater is silicate weathering such as feldspar and dissolution of carbonate rocks such as calcite [CaCO_3] and dolomite [$\text{CaMg}(\text{CO}_3)_2$] in the aquifers [69] and expressed in Eqs. 6 and 7.

Organic decay and root respiration Formation of carbonic acid:



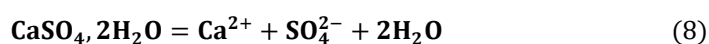
(6)

Calcite dissolution :



HCO_3^- concentrations are in the range of 129.32 to 283.04 mg/L, with an average of 187.6 mg/L. According to the spatial distribution map of bicarbonate in the study area (Figure 6c), all samples have HCO_3^- concentration which exceeded the value guide of 120 mg/L [57]. The highest bicarbonate concentration (283.04 mg/L) was recorded at F-31 in the northeastern parts of the study area, and the lowest is 129.32 mg/L at F-16 in the southwestern parts of the study area (Figure 6c).

The presence of sulfate ions in water is linked to the dissolution of gypsum formations, the degradation of organic matter in the soil, and anthropogenic input (agricultural origin), expressed in Eq. 8:



Groundwater with a high concentration of Cl^- and sulfate could affect the corrosion phenomena and water distribution network systems [70]. The values of sulfates in water samples varied from 571.43 to 3028.57 mg/L, with an average of 1636.22 mg/L (Table 1). According to the spatial variation map (Figure 6g), it indicates that the highest concentrations of SO_4^{2-} were observed in the southwestern parts of the study area. Moreover, all groundwater samples have SO_4^{2-} concentrations that are higher than the value guide of [57] drinking water quality guidelines (250 mg/L). The elevated SO_4^{2-} contents, as presented in the spatial distribution map (Figure 6g), may be attributed to the dissolution of gypsum minerals and other anthropogenic influences.

The origin of chlorine is mainly linked to the dissolution of salt formations. Evaporites are the main source of this element. The effect of endorheic basins, the salting of roads, and wastewater discharges can also be the cause of this element [5]. In unconfined aquifers, the chloride concentration is directly related to the chloride content of precipitation. The concentrations measured in these systems depend on the lithology. In confined aquifers, high chloride contents are to be expected in the presence of evaporitic formations rich in chlorine [71]. Chloride concentrations for all groundwater samples ranged from 106.5–1462.6 mg/L, with an average value of 462.07 mg/L (Table 1). The highest contents (1462.6 mg/L) were registered in F-11 in the West-center part of the study area (Figure 6d). 74 % of the groundwater samples have a Cl^- concentration above the value guide of [57] drinking water quality guidelines. The high chloride concentrations in the groundwater samples, in particular of the west-center part of the study area, may be due to salt inputs from evaporitic formations and probably from the agri-food industry in the region or linked to urbanization through wastewater discharges.

Nitrates can have several origins. The main factors that determine the high concentration of NO_3^- are anthropogenic activities such as extensively irrigated with the excess application of inorganic nitrogenous fertilizers, return flow irrigation, and domestic and industrial discharges [5,72]. Pollution by nitrate is a matter of high concern as it can negatively affect ecosystems [73]. NO_3^- ion is a familiar pollutant in water [74]. The maximum value was obtained at F-6 at 153.44 mg/L and the lowest of 0.2 mg/L at F-12, with an average value of 37.13 mg/L in the groundwater of the study area (Table 1). For the spatial variation map (Figure 6h), the highest contents were observed in the center parts of the study area, which coincides with village Lioua, and agricultural areas.

As shown in Figure 7, cations are plotted in zones B and A, indicating that the groundwater in the studied area is mainly of the calcium type and no dominant type. For anions, samples are mostly in zone F, which has a strong prevalence of sulfate type. All groundwater samples in the study area are plotted in zone 1, such SO_4^{2-} , Ca^{2+} , and Mg^{2+} are the major ions. The examination of the molar concentrations of different elements in the area shows that the cations evolve as follows: $\text{Ca}^{2+} > \text{Mg}^{2+} > \text{Na}^+ > \text{K}^+$ while the anions evolve in the following manner: $\text{SO}_4^{2-} > \text{Cl}^- > \text{HCO}_3^- > \text{NO}_3^-$. The chemical profile is calcium and magnesium sulfate facies due to the dissolution of evaporitic formations. The distribution of the main ions (Ca^{2+} , Mg^{2+} , and SO_4^{2-}) is highly influenced by the lithology of the region and is due to anthropogenic sources such as irrigation water quality and uncontrolled fertilization. Both calcium and magnesium can come from the dissolution of calcium or magnesium sulfates. The transition from one dominant ratio to another can be done by dilution after mixing or precipitation of one of the ions. Two distinct origins of SO_4^{2-} are clearly highlighted: the first one is from the breakdown of organic matters in the soil and from the addition of leachable sulfates in fertilizers of the intensively cultivated areas in Lioua plain, and the second one is the dissolution of gypsum [78]. The presence of the evaporate sequence allows the dissolution of gypsum according to the equation (8) [79].

Concerning the results obtained from the Chadha's diagram, is similar to the results obtained from the piper plot (Figure 7). Such water has permanent hardness and acquire their mineralization in the process of reverse ion exchange. Therefore, when irrigated, they do not deposit residual sodium carbonate.

According to the figure 9 which represent the Gibbs diagram, the Lioua region belongs to an arid climatic zone, and the evaporation rate is high, which is responsible for the diversion of the plots to the evaporation dominance zone (Figure 9). On the other hand, human activities can also influence the hydrochemical evolution processes of groundwater, which cannot be interpreted by Gibbs diagram [82]. However, it is clear that the enhancement of water levels induced by the intensification of irrigation and effective rainfall associated with the shallow water depth in the region, evaporation has become the main driver of ion concentration. In addition, the upper unsaturated but moist matrix especially at the approach of the saturated zone is rich in evaporites, which leads to the precipitation of evaporites by evaporation that are eventually leached into the saturated zone. Consequently, all this leads to an increase in salinity (TDS max = 7145 mg/L), as groundwater evaporation is more intense as the water level rises and sulfate groundwater is more influenced by evaporation than bicarbonate groundwater [5]. This result is supported by other studies that confirmed the sulfate type of groundwater undergoing intense evaporation in the alluvial plain [83].

As shown in Figure 10a, both reverse ion exchange and ion exchange are affecting the aquifer chemistry in the study area of Lioua. The samples close to the 1:1 line, indicating that the dissolutions of calcite, dolomite, and gypsum are the prevalent reactions in the system of the study region. Those under the 1:1 line exhibit the processes of ion exchange, where Ca^{2+} is retained in the soil and the Na^+ is returned in the groundwater. Inversely, those above the line 1:1 exhibit the reverse ion exchange, where the Ca^{2+} is emitted into the groundwater and the Na^+ is retained in the soil. The samples above the line 1:1, are enriched in calcium and magnesium. Therefore, this suggest that the dissolution of Ca^{2+} and Mg^{2+} from evaporites is greater than from carbonates. The Ca^{2+} , Mg^{2+} and SO_4^{2-} contents are more related to the dissolution of evaporites, essentially gypsum, anhydrite and magnesium sulfate. According to Appelo and Postma [85], the presence of sulfates in large amounts in groundwater could also be attributed to the dissolution of the anhydrite and pyrite. On an average, the contribution of direct ion exchange and reverse ion exchange reaction is almost equal.

Figure 10b shows the ratio of $\text{Ca}^{2+}/\text{SO}_4^{2-}$ and $\text{Mg}^{2+}/\text{SO}_4^{2-}$. A high correlation between Ca^{2+} and SO_4^{2-} was found, with a value correlation coefficient of 0.74, and that of Mg^{2+} and SO_4^{2-} is 0.67. In the scatter plot between SO_4^{2-} and Ca^{2+} (Figure 10b), most of the samples were below the equiline (1:1), indicating the gypsum and anhydrite dissolution in groundwater [86]. The far samples from line 1:1 indicate another source of SO_4^{2-} , such as mineral weathering, ion exchange reactions, and the agricultural activities.

In addition, the ion exchange mechanism commonly used to determine the occurrence of cation exchange processes is studied by plotting $(\text{Ca}^{2+} + \text{Mg}^{2+} - \text{HCO}_3^- - \text{SO}_4^{2-})$ versus $(\text{Na}^+ - \text{Cl}^-)$ [84]. It is agreed that the excess $(\text{Ca}^{2+} + \text{Mg}^{2+})$ could be related to sources other than carbonate and gypsum. Most water samples are close to the $y = -X$ line (Figure 10c) and only a few points deviate from this relationship, indicating that cation exchange plays a nontrivial role in controlling the hydrochemical components of groundwater. Excess Ca^{2+} can exchange Na^+ from aquifer minerals, resulting in increased Na^+ in the groundwater.

In order to recognize the ion exchange process between groundwater and aquifer minerals, chloroalkalinity was applied. In general, Na^+ and K^+ in groundwater are exchanged with Ca^{2+} and Mg^{2+} in the aquifer matrix. When there is an exchange between Ca^{2+} or Mg^{2+} in the groundwater with Na^+ and K^+ in the aquifer material, both chloroalkaline indices (CAI-I and CAI-II) are negative and if there is a reverse ion exchange, both indices will be positive. In the Lioua system, Na^+ and K^+ decrease in the groundwater, representing direct ion exchange. Most CAI values for groundwater samples in CAI-1 and CAI-2 were both negative (Figure 10d), while only seven samples were positive. Therefore, exchange of Ca^{2+} and Mg^{2+} with Na^+ and K^+ is the predominant cation exchange process.

In our results, since Mg^{2+} concentrations in water are only likely to be increased as Mg^{2+} is liberated from ferromagnesium minerals in the bedrock during chemical weathering, it is minor component of soil salts and is not precipitated in the early stages of evaporation of low silica water [87–89]. Therefore, the concentration of magnesium will not be changed by the influence of soil salt leaching and salt precipitation during the early stages of water evaporation. In terms of $\text{Mg}^{2+}/\text{Cations}$ pattern (Figure 10e), the groundwater in the study area is a single rocky zone plot. The samples had average $\text{Mg}^{2+}/\text{Na}^+$ ratios and average $\text{Mg}^{2+}/\text{Ca}^{2+}$ ratios and were located in the rock-dominated zone (Figure 10e). This plot indicates that major ions in this study area differ from water-rock interactions, while soil-salt leaching could be a subdominant process and evaporation only a minor process.

The natural processes responsible for major solutes in natural water are probably dominated by mineral dissolution [89]. Gaillardet et al. [90] proposed using a Na-normalized molar ratio to reflect different hydrochemical reactions under non-mixed conditions. The diagrams of Na-normalized Ca^{2+} versus Mg^{2+} plot and Na-normalized Ca^{2+} versus HCO_3^- show that the natural water samples in Lioua plain are influenced by water-rock interactions such as silicate weathering and slightly carbonate dissolution. Figure 10f shows that silicate weathering was the major process to control the groundwater solute concentration.

Results from PCA are more efficient when the number of factors is small [94]. The parameter loading for the 3 components from the PCA of the data set is given in Table 3. The factorial analysis revealed that factor 1 explains the greatest amount of the variance (68.72 %) and is characterized by highly negative loadings in EC, TDS, Cl^- , Na^+ , Mg^{2+} , Ca^{2+} , K^+ , and SO_4^{2-} , which were -0.98 , -0.97 , -0.94 , -0.93 , -0.91 , -0.89 , -0.70 and -0.82 , respectively (Table 3). They are controlled by lithologic factors and various hydrogeochemical processes resulting in high EC and TDS scores (mineralized water). On the F1-F2 factorial plan (Figure 11), the factor F1 is determined negatively by TDS, EC, Cl^- , Na^+ , Mg^{2+} ,

SO_4^{2-} , K^+ , and Ca^{2+} , which highlight the origin of the salinity by weathering of silicate, limestone, halite and gypsum, pyrite dissolution, and various ion exchange processes in the water system [95]. Therefore, the factor can be termed a salinization factor.

Factor 2 explains 11.96 % of the total variance of the dataset and shows significant negative loadings in NO_3^- and HCO_3^- (Figure 11), which were -0.66 and -0.64. This indicates that the element does not influence the total mineralization of the water and predicts the carbonate origin for HCO_3^- by weathering of the carbonates and could reflect the influence of acid-base equilibrium conditions on groundwater chemistry [96].

On the factorial plane F1-F3, factor 3 explains 8.89 % of the total variance of the dataset (Figure 11) and shows significant negative loading in NO_3^- (-0.59), which predicts the association of this factor with chemical fertilizers, animal waste, crop residues and mineralization of soil and non-agricultural sources such as septic tanks or deep water mixing with surface water. As we know, large amounts of fertilizer, such as urea and commercial composite, have been applied for a long time, which are a major constituent resulting from the return flow from the development of irrigation. Under toxic conditions, the main component of fertilizers, NH_4^+ , is easily oxidized to NO_3^- by the nitrification process [97], as reported in the equation (9).



The Dendrogram of the 10 physicochemical parameters (Ca^{2+} , Mg^{2+} , Na^+ , K^+ , Cl^- , HCO_3^- , SO_4^{2-} , NO_3^- , EC and TDS) can be divided into three main groups (Figure 12) and reveals that TDS and EC can be the major elements of distinction between parameters. G1 reveals a close association with SO_4^{2-} , K^+ , Ca^{2+} , and TDS, which reflects the major predominance of these elements in the chemical composition of groundwater in the region (sulfates and anhydride, calcium sulfates). This is clearly visible by the calcium sulfate chemical facies. Similarly, group G1 shows a distant association between K^+ and Ca^{2+} , which reflects the probably different origins of these two elements. G2 reveals a close association between Na^+ , Cl^- , Mg^{2+} , and EC, which reflects the major participation of salts and chlorides in the electrical conductivity of water. The G1 and G2 united reflect the dominance of the lithological factor in the overall mineralization of the waters of the Plio-Quaternary surface aquifer of Lioua. G3 shows the dissociation of bicarbonates and nitrates from other chemical elements present in groundwater, which reflects the different origins of these two elements, carbonated for HCO_3^- and anthropogenic for NO_3^- . It should be noted that these analyzes corroborate well with the results of the analysis of the correlation matrix between variables.

The autocorrelation functions of pH recorded a high value. This is an indicator of the uncorrelated characteristics of the pH with other parameters [100]. On the other hand, the autocorrelation function of Mg^{2+} , SO_4^{2-} , Cl^- , Na^+ , K^+ , and EC shows a sinusoidal pattern. Thus, these variables have strong interrelationships with a constant period of investigation. However, the mean autocorrelation coefficients decrease slowly from 0.7 to -0.3 for pH and Ca^{2+} . Obtained results show a mean linear interrelationship of EC, Mg^{2+} , Na^+ , K^+ , Cl^- and SO_4^{2-} autocorrelation. While, for the parameters' NO_3^- and HCO_3^- is an indicator of the uncorrelated characteristics with other parameters. In the study area, the NO_3^- resulted from the human activity fertilizer and domestic sewage. However, HCO_3^- resulted from the carbonate facies outcrops. [101] also reported these results.

Spectral density functions of all the hydrochemical variables are shown that the salinity was affected by these elements and that EC played a more vital role in the groundwater quality. The preparation of activated carbon from wooden or other materials has helped to receive efficient adsorbents for the removal of pollutants from water [102, 103].

pH, Ca^{2+} , HCO_3^- and NO_3^- exhibit multiple peaks, which means that several distinct cyclic mechanisms are present [104]. The multiple peaks of these elements resulted from the human activity fertilizer, the carbonate facies outcrops, and domestic sewage [105].

5. Conclusions

In this study, the hydrochemistry of Lioua's groundwater in Algeria's Lower Sahara was experimentally explored using chemometrics methods. The aim was to deduce the geochemical processes influencing the chemical composition and to determine chemical elements' origins. The Multivariate statistical analysis and time series approaches were used. Principal component analysis (PCA) and cluster analysis (CA) are applied when autocorrelation analysis supplemented by simple spectral density analysis was used as time series methods. The main finding obtained is that: PCA displays three main factors explaining a total variance (TV) of 85.01 %. Factors 1, 2, and 3 are 68.72, 11.96, and 8.89 % of TV. Those results indicate that the dissolution of evaporated mineral deposits, water-rock interaction, and evaporation process are the geochemical processes influencing the chemical composition.

In the CA, tree groups are controlled by TDS and EC. G1 reveals a close association with SO_4^{2-} , K^+ , Ca^{2+} , and TDS, and G2 reveals a close association between Na^+ , Cl^- , Mg^{2+} and EC. G3 shows the dissociation of bicarbonates HCO_3^- and NO_3^- from other chemical elements. These results indicate that Groundwater exhibits, also, two bipolar characteristics, one recorded with negative and positive charges on pH and on Ca^{2+} and another recorded only with negative charges on HCO_3^- and NO_3^- .

The autocorrelation analysis shows a linear interrelationship of EC, Mg^{2+} , Na^+ , K^+ , Cl^- , and SO_4^{2-} . While for NO_3^- and HCO_3^- it indicates uncorrelated characteristics with other parameters. In addition, SDA shows that the correlograms of Mg^{2+} , Na^+ , K^+ , Cl^- , and SO_4^{2-} have a similar trend with EC. However, pH, Ca^{2+} , HCO_3^- and NO_3^- exhibit multiple peaks possibly related to the existence of several distinct cyclic mechanisms. The major participation of salts and chlorides is in the electrical conductivity of water. The combination of autocorrelation analysis and simple spectral density analysis results confirm the following findings:

- The dominance of the lithological factor in the overall mineralization of the of Plio-Quaternary surface aquifer waters.
- The origins of HCO_3^- and NO_3^- are different. Indeed, carbonated for HCO_3^- has a carbonate origin, whereas NO_3^- has an anthropogenic origin.
- The salinity was affected by Mg^{2+} , SO_4^{2-} , Cl^- , Na^+ , K^+ , and EC.
- Ca^{2+} , HCO_3^- and NO_3^- are resulted from human activity fertilizers, the carbonate facies outcrops, and domestic sewage.

The results presented in this study demonstrated the potential of the chemometrics methods applied to hydrochemistry.

Author Contributions: Conceptualization, A.A. and A.G.; methodology, A.G. J.B, A.E.K. and I.Z.; software, H.A.A.; validation, A.A., A.G. and H.A.A.; formal analysis, A.A. and A.G.; investigation, A.A.; resources, A.A. and A.G.; data curation, S.B. and A.E.K.; writing—original draft preparation, A.G. and H.A.A.; writing—review and editing, H.A.A., S.B., J.B, I.Z. and A.E.K.; visualization, S.B, J.B and I.Z.; supervision, A.E.K.; project administration, A.A.; funding acquisition, H.A.A., J.B, A.E.K. and I.Z. All authors have read and agreed to the published version of the manuscript.

Funding: The work was supported by the PASIFIC program GeoReco project funding from the European Union's Horizon2020 research and innovation programme under the Marie Skłodowska-Curie grant agreement No.847639 and from the Ministry of Education and Science. A.E.Krauklis' contribution was supported by the LZIP Project Nr. lzp-2021/1-0090 CircleP. The research was conducted under the collaborative project 'Identifying best available technologies for decentralized wastewater treatment and resource recovery for India (SARASWATI 2.0)'; co-funding from the European Commission within the Horizon 2020 Framework Programme (grant agreement number 821427) and from the Government of India (Department for Science and Technology) is gratefully acknowledged and SLTKT20427 "Sewage sludge treatment from heavy metals, emerging pollutants and recovery of metals by fungi" and by PLTKT ARENG53. This study was also supported by the MESRS (Ministry of Higher Education and Scientific Research of Algeria) and the DGRSDT (General Direction).

Informed Consent Statement: Not applicable.

Data Availability Statement: The datasets used and/or analyzed during the current study are available from the corresponding author upon a reasonable request.

Acknowledgments: Many thanks are addressed to the MESRS and the DGRSDT. Andrey is grateful to Oksana.

Conflicts of Interest: The authors declare that they have no competing interests. The funders had no role in the design of the study; in the collection, analyses, or interpretation of data; in the writing of the manuscript, or in the decision to publish the results

References

1. Burlakovs, J.; Lacis, D. The Developmental Trends of Groundwater Horizon Surface Depression and Sea Water Intrusion Impact in Liepaja City. 5.
2. Gul, S.; Gul, H.; Gul, M.; Khattak, R.; Rukh, G.; Khan, M.S.; Aouissi, H.A. Enhanced Adsorption of Rhodamine B on Biomass of Cypress/False Cypress (*Chamaecyparis Lawsoniana*) Fruit: Optimization and Kinetic Study. *Water* 2022, 14, 2987, doi:10.3390/w14192987.
3. Travi, Y. Hydrogéologie et hydrochimie des aquifères du Sénégal. *Hydrogéochimie du fluor dans les eaux souterraines. Sciences Géologiques, bulletins et mémoires* 1993, 95.
4. Xu, P.; Zhang, Q.; Qian, H.; Zheng, L. Spatial Distribution Characteristics of Irrigation Water Quality Assessment in the Central-Western Guanzhong Basin, China. *IOP Conf. Ser.: Earth Environ. Sci.* 2021, 647, 012143, doi:10.1088/1755-1315/647/1/012143.
5. Athamena, A.; Menani, M.R. Nitrogen Flux and Hydrochemical Characteristics of the Calcareous Aquifer of the Zana Plain, North East of Algeria. *Arab J Geosci* 2018, 11, 356, doi:10.1007/s12517-018-3681-5.
6. Vincevica-Gaile, Z.; Sachpazidou, V.; Bisters, V.; Klavins, M.; Anne, O.; Grinfelde, I.; Hanc, E.; Hogland, W.; Ibrahim, M.A.; Jani, Y.; et al. Applying Macroalgal Biomass as an Energy Source: Utility of the Baltic Sea Beach Wrack for Thermochemical Conversion. *Sustainability* 2022, 14, 13712, doi:10.3390/su142113712.
7. Boudoukha, A.; Athamena, M. Caractérisation des eaux thermales de l'ensemble Sud sétifien. *Est algérien. rseau* 2012, 25, 103–118, doi:10.7202/1011602ar.
8. Belalite; Menani, M.R.; Athamena, A. Calculation of Water Needs of the Main Crops and Water Resources Available in a Semi-Arid Climate, Case of Zana-Gadaïne Plain, Northeastern Algeria. *Algerian Journal of Environmental Science and Technology* 2022, 8.
9. Gaagai, A.; Aouissi, H.A.; Krauklis, A.E.; Burlakovs, J.; Athamena, A.; Zekker, I.; Boudoukha, A.; Benaabidate, L.; Chenchouni, H. Modeling and Risk Analysis of Dam-Break Flooding in a Semi-Arid Montane Watershed: A Case Study of the Yabous Dam, Northeastern Algeria. *Water* 2022, 14, 767, doi:10.3390/w14050767.

10. Fahad N. Al-Barakah; Aly, A.A.; Abaakhel, E.H.S.; Al-Rizkid, A.M.; Alghamdi, A.G.; Al-Sewailem, M.S. Comparison and Hydrochemical Characterization of Groundwater Resources in the Arabian Peninsula: A Case Study of Al-Baha and Al-Qassim in Saudi Arabia. *Water Resour* 2020, 47, 877–891, doi:10.1134/S0097807820050073.
11. Mfonka, Z.; Kpoumié, A.; Ngouh, A.N.; Mouncherou, O.F.; Nsangou, D.; Rakotondrabe, F.; Takounjou, A.F.; Zammouri, M.; Ngoupayou, J.R.N.; Ndjigui, P.-D. Water Quality Assessment in the Bamoun Plateau, Western-Cameroon: Hydrogeochemical Modelling and Multivariate Statistical Analysis Approach. *Journal of Water Resource and Protection* 2021, 13, 112–138, doi:10.4236/jwarp.2021.132007.
12. Awasthi, A.; Rishi, M.S.; Panjgotra, S. Groundwater Quality Assessment for Drinking and Industrial Purposes in Transboundary Aquifers of Gurdaspur District, Punjab, India. *International Journal of Environmental Analytical Chemistry* 2021, 0, 1–15, doi:10.1080/03067319.2021.2020766.
13. Khelifi, W.; Bencedira, S.; Azab, M.; Riaz, M.S.; Abdallah, M.; Abdel Baki, Z.; Krauklis, A.E.; Aouissi, H.A. Conservation Environments' Effect on the Compressive Strength Behaviour of Wood–Concrete Composites. *Materials* 2022, 15, 3572, doi:10.3390/ma15103572.
14. Singh, P.; Rishi, M.S.; Kaur, L. Multi-Parametric Analysis of Groundwater Quality to Assess Human Health Risk and Hydrogeochemical Processes in an Agriculturally Intensive Alluvial Aquifer of Northwest India. *International Journal of Environmental Analytical Chemistry* 2022, 0, 1–19, doi:10.1080/03067319.2022.2064750.
15. Krauklis, A.E.; Kreicbergs, I.; Dreyer, I. Modified Ginstling-Brounshtein Model for Wet Precipitation Synthesis of Hydroxyapatite: Analytical and Experimental Study. *Acta Bioeng Biomech* 2018, 20, 47–57.
16. Belhadj, M.Z.; Boudoukha, A.; Amroune, A.; Gaagai, A.; Ziani, D. STATISTICAL CHARACTERIZATION OF GROUNDWATER QUALITY OF THE NORTHERN AREA OF THE BASIN OF HODNA, M'SILA. SOUTHEASTERN ALGERIA. *LARHYSS Journal* P-ISSN 1112-3680 / E-ISSN 2521-9782 2017, 177–194.
17. Herojeet, R.; Rishi, M.S.; Lata, R.; Dolma, K. Quality Characterization and Pollution Source Identification of Surface Water Using Multivariate Statistical Techniques, Nalagarh Valley, Himachal Pradesh, India. *Appl Water Sci* 2017, 7, 2137–2156, doi:10.1007/s13201-017-0600-y.
18. Rajkumar, H.; Naik, P.K.; Rishi, M.S. Evaluation of Heavy Metal Contamination in Soil Using Geochemical Indexing Approaches and Chemometric Techniques. *Int. J. Environ. Sci. Technol.* 2019, 16, 7467–7486, doi:10.1007/s13762-018-2081-4.
19. Aouissi, H.A.; Petrișor, A.-I.; Ababsa, M.; Boștenaru-Dan, M.; Tourki, M.; Bouslama, Z. Influence of Land Use on Avian Diversity in North African Urban Environments. *Land* 2021, 10, 434, doi:10.3390/land10040434.
20. Belkhiri, L.; Narany, T.S. Using Multivariate Statistical Analysis, Geostatistical Techniques and Structural Equation Modeling to Identify Spatial Variability of Groundwater Quality. *Water Resour Manage* 2015, 29, 2073–2089, doi:10.1007/s11269-015-0929-7.
21. Gaagai, A.; Boudoukha, A.; Boumezbeur, A.; Benaabidate, L. Hydrochemical Characterization of Surface Water in the Babar Watershed (Algeria) Using Environmetric Techniques and Time Series Analysis. *International Journal of River Basin Management* 2017, 15, 361–372.
22. Meng, S.X.; Maynard, J.B. Use of Statistical Analysis to Formulate Conceptual Models of Geochemical Behavior: Water Chemical Data from the Botucatu Aquifer Is Sao Paulo State, Brazil. *Journal of hydrology* 2001.
23. Farnham, I.M.; Stetzenbach, K.J.; Singh, A.K.; Johannesson, K.H. Deciphering Groundwater Flow Systems in Oasis Valley, Nevada, Using Trace Element Chemistry, Multivariate Statistics, and Geographical Information System. *Mathematical Geology* 2000, 32, 943–968, doi:10.1023/A:1007522519268.

24. Roubil, A.; El Ouali, A.; Bülbül, A.; Lahrach, A.; Mudry, J.; Mamouch, Y.; Essahlaoui, A.; El Hmaidi, A.; El Ouali, A. Groundwater Hydrochemical and Isotopic Evolution from High Atlas Jurassic Limestones to Errachidia Cretaceous Basin (Southeastern Morocco). *Water* 2022, 14, 1747, doi:10.3390/w14111747.
25. Lu, Y.; Tang, C.; Chen, J.; Chen, J. Groundwater Recharge and Hydrogeochemical Evolution in Leizhou Peninsula, China. *Journal of Chemistry* 2015, 2015, e427579, doi:10.1155/2015/427579.
26. Shen, F.; Yang, L.; He, X.; Zhou, C.; Adams, J.M. Understanding the Spatial–Temporal Variation of Human Footprint in Jiangsu Province, China, Its Anthropogenic and Natural Drivers and Potential Implications. *Sci Rep* 2020, 10, 13316, doi:10.1038/s41598-020-70088-w.
27. Wan, L.; Li, Y.C. Time Series Trend Analysis and Prediction of Water Quality in a Managed Canal System, Florida (USA). *IOP Conf. Ser.: Earth Environ. Sci.* 2018, 191, 012013, doi:10.1088/1755-1315/191/1/012013.
28. Loucks, D.P.; van Beek, E. Water Resources Planning and Management: An Overview. In *Water Resource Systems Planning and Management: An Introduction to Methods, Models, and Applications*; Loucks, D.P., van Beek, E., Eds.; Springer International Publishing: Cham, 2017; pp. 1–49 ISBN 978-3-319-44234-1.
29. Aouissi, H.A.; Ababsa, M.; Gaagai, A.; Bouslama, Z.; Farhi, Y.; Chenchouni, H. Does Melanin-Based Plumage Coloration Reflect Health Status of Free-Living Birds in Urban Environments? *Avian Research* 2021, 12, 45, doi:10.1186/s40657-021-00280-7.
30. Koull, N.; Helimi, S.; Mihoub, A.; Mokhtari, S.; Kherraze, M.E.; Aouissi, H.A.; Koull, N.; Helimi, S.; Mihoub, A.; Mokhtari, S.; et al. Integración de SIG y Análisis Jerárquico Multi-Criterio Para Analizar La Idoneidad de La Tierra Para Los Cereales En La Zona Árida de Argelia. *International journal of agriculture and natural resources* 2022, 49, 36–50, doi:10.7764/ijanr.v49i1.2323.
31. Teegavarapu, R.S.V. Chapter 1 - Methods for Analysis of Trends and Changes in Hydroclimatological Time-Series. In *Trends and Changes in Hydroclimatic Variables*; Teegavarapu, R., Ed.; Elsevier, 2019; pp. 1–89 ISBN 978-0-12-810985-4.
32. Reghunath, R.; Murthy, T.R.S.; Raghavan, B.R. The Utility of Multivariate Statistical Techniques in Hydrogeochemical Studies: An Example from Karnataka, India. *Water Research* 2002, 36, 2437–2442, doi:10.1016/S0043-1354(01)00490-0.
33. Chorfi, A.; Hafid, H.; Baaloudj, A.; Rizi, H.; Aouissi, H.A.; Chaib, S.; Ababsa, M.; Allaoua, N.; Houhamdi, M. Characterization and Diversity of Macroin-Vertebrates in Groundwater in the Region of Souk-Ahras (North-East of Algeria). *Ekológia (Bratislava)* 2022, 41, 219–227, doi:10.2478/eko-2022-0022.
34. Ahcène, S.; Bachir, H.; Bourafai, S. Hydrochemical Characteristics of Aquifers and Their Predicted Impact on Soil Properties in Biskra Region, Algeria. *Egyptian Journal of Agricultural Research* 2021, 99, 205–220, doi:10.21608/ejar.2021.56750.1068.
35. Guettaia, S.; Hacini, M.; Boudjema, A.; Zahrouna, A. Vulnerability Assessment of an Aquifer in an Arid Environment and Comparison of the Applied Methods: Case of the Mio-Plio-Quaternary Aquifer. *Energy Procedia* 2017, 119, 482–489, doi:10.1016/j.egypro.2017.07.057.
36. Obeidat, M.; Awawdeh, M. Assessment of Groundwater Quality in the Area Surrounding Al- Zaatari Camp, Jordan, Using Cluster Analysis and Water Quality Index (WQI). 2021, 11.
37. Standard Methods for the Examination of Water & Wastewater, Centennial Edition; Eaton, A.D., Clesceri, L.S., Rice, E.W., Greenberg, A.E., Franson, M.A.H., Eds.; 21st edition.; Amer Public Health Assn: Washington, DC, 2005; ISBN 978-0-87553-047-5.

-
38. Singh, G.; Rishi, M.S.; Herojeet, R.; Kaur, L.; Sharma, K. Evaluation of Groundwater Quality and Human Health Risks from Fluoride and Nitrate in Semi-Arid Region of Northern India. *Environ Geochem Health* 2020, 42, 1833–1862, doi:10.1007/s10653-019-00449-6.
 39. Singh, G.; Rishi, M.S.; Herojeet, R.; Kaur, L.; Priyanka; Sharma, K. Multivariate Analysis and Geochemical Signatures of Groundwater in the Agricultural Dominated Taluks of Jalandhar District, Punjab, India. *Journal of Geochemical Exploration* 2020, 208, 106395, doi:10.1016/j.gexplo.2019.106395.
 40. Simeonov, V.; Stratis, J.A.; Samara, C.; Zachariadis, G.; Voutsas, D.; Anthemidis, A.; Sofoniou, M.; Kouimtzis, Th. Assessment of the Surface Water Quality in Northern Greece. *Water Research* 2003, 37, 4119–4124, doi:10.1016/S0043-1354(03)00398-1.
 41. Singh, K.P.; Malik, A.; Sinha, S. Water Quality Assessment and Apportionment of Pollution Sources of Gomti River (India) Using Multivariate Statistical Techniques—a Case Study. *Analytica Chimica Acta* 2005, 538, 355–374, doi:10.1016/j.aca.2005.02.006.
 42. Vieira, J.S.; Pires, J.C.M.; Martins, F.G.; Vilar, V.J.P.; Boaventura, R.A.R.; Botelho, C.M.S. Surface Water Quality Assessment of Lis River Using Multivariate Statistical Methods. *Water Air Soil Pollut* 2012, 223, 5549–5561, doi:10.1007/s11270-012-1267-5.
 43. Simeonov, V.; Simeonova, P.; Tzimou-Tsitouridou, R. Chemometric Quality Assessment of Surface Waters: Two Case Studies. *Chemia i Inżynieria Ekologiczna* 2004, 449–469.
 44. Yang, K.; Xu, C.; Chi, M.; Wang, P. Analytical Analysis of the Groundwater Drawdown Difference Induced by Foundation Pit Dewatering with a Suspended Waterproof Curtain. *Applied Sciences* 2022, 12, 10301, doi:10.3390/app122010301.
 45. Kaiser, H.F. The Application of Electronic Computers to Factor Analysis. *Educational and Psychological Measurement* 1960, 20, 141–151, doi:10.1177/001316446002000116.
 46. Devkota, J.U. Multivariate Analysis of COVID-19 for Countries with Limited and Scarce Data: Examples from Nepal. *J Environ Public Health* 2021, 2021, 8813505, doi:10.1155/2021/8813505.
 47. Wai, W.W.; AlKarkhi, A.F.M.; Easa, A.M. Comparing Biosorbent Ability of Modified Citrus and Durian Rind Pectin. *Carbohydrate Polymers* 2010, 79, 584–589, doi:10.1016/j.carbpol.2009.09.018.
 48. Swanson, S.K.; Bahr, J.M.; Schwar, M.T.; Potter, K.W. Two-Way Cluster Analysis of Geochemical Data to Constrain Spring Source Waters. *Chemical Geology* 2001, 179, 73–91, doi:10.1016/S0009-2541(01)00316-3.
 49. Danielsson, Å.; Cato, I.; Carman, R.; Rahm, L. Spatial Clustering of Metals in the Sediments of the Skagerrak/Kattegat. *Applied Geochemistry* 1999, 14, 689–706, doi:10.1016/S0883-2927(99)00003-7.
 50. Fovell, R.G.; Fovell, M.-Y.C. Climate Zones of the Conterminous United States Defined Using Cluster Analysis. *Journal of Climate* 1993, 6, 2103–2135, doi:10.1175/1520-0442(1993)006<2103:CZOTCU>2.0.CO;2.
 51. Taheri Tizro, A.; Ghashghaie, M.; Georgiou, P.; Voudouris, K. Time Series Analysis of Water Quality Parameters. *Journal of Applied Research in Water and Wastewater* 2014, 1, 40–50.
 52. Mangin, A. The use of autocorrelation and spectral analyses to obtain a better understanding of hydrological systems. *Journal of hydrology* 1984.
 53. Padilla, A.; Pulido-Bosch, A.; Mangin, A. Relative Importance of Baseflow and Quickflow from Hydrographs of Karst Spring. *Groundwater* 1994, 32, 267–277, doi:10.1111/j.1745-6584.1994.tb00641.x.

54. Chung, S.Y.; Venkatramanan, S.; Park, N.; Rajesh, R.; Ramkumar, T.; Kim, B.W. An Assessment of Selected Hydrochemical Parameter Trend of the Nakdong River Water in South Korea, Using Time Series Analyses and PCA. *Environ Monit Assess* 2015, 187, 4192, doi:10.1007/s10661-014-4192-9.
55. Lee, J.-Y.; Lee, K.-K. Use of Hydrologic Time Series Data for Identification of Recharge Mechanism in a Fractured Bedrock Aquifer System. *Journal of Hydrology* 2000, 229, 190–201, doi:10.1016/S0022-1694(00)00158-X.
56. Box, G.E.P. *Time Series Analysis: Forecasting and Control*; 3rd ed.; Prentice Hall: Englewood Cliffs, N.J, 1994; ISBN 978-0-13-060774-4.
57. WHO Guidelines for Drinking-water Quality; 3rd ed.; 2017; Vol. 1; ISBN ISBN 978-92-4-154995-0.
58. Amin, M.; Yousuf, M.; Ahmad, N.; Attaullah, M.; Ahmad, S.; Zekker, I.; Latif, M.; Buner, I.D.; Khan, A.A.; Ali, H.; et al. Application of Alkaline Phosphatase to Assess the Health of *Oreochromis Niloticus* Exposed to Organophosphates and Synthetic Pyrethroid Pesticides In Vivo. *Journal of Hazardous, Toxic, and Radioactive Waste* 2022, 26, 04022029, doi:10.1061/(ASCE)HZ.2153-5515.0000714.
59. Grochowska, J. Assessment of Water Buffer Capacity of Two Morphometrically Different, Degraded, Urban Lakes. *Water* 2020, 12, 1512, doi:10.3390/w12051512.
60. Cocomazzi, G.; Grieco, G.; Sinojmeri, A.; Cavallo, A.; Bussolesi, M.; Ferrari, E.S.; Destefanis, E. Buffering Copper Tailings Acid Mine Drainage: Modeling and Testing at Fushë Arrëz Flotation Plant, Albania. *Water* 2022, 14, 2398, doi:10.3390/w14152398.
61. Ghodbane, M.; Benaabidate, L.; Boudoukha, A.; Gaagai, A.; Adjissi, O.; Chaib, W.; Aouissi, H.A. *Journal of Water and Land Development* 2022, doi:10.24425/JWLD.2022.141549.
62. R. J. Davis, S.N. and D. *Hydrogeology*, 1966, 463 Pages with Illustrations.; John Wiley & Sons, 1966;
63. Tang, H.; Zhong, H.; Pan, Y.; Zhou, Q.; Huo, Z.; Chu, W.; Xu, B. A New Group of Heterocyclic Nitrogenous Disinfection Byproducts (DBPs) in Drinking Water: Role of Extraction PH in Unknown DBP Exploration. *Environ. Sci. Technol.* 2021, 55, 6764–6772, doi:10.1021/acs.est.1c00078.
64. Krauklis, A.E.; Aouissi, H.A.; Bencedira, S.; Burlakovs, J.; Zekker, I.; Bute, I.; Klavins, M. Influence of Environmental Parameters and Fiber Orientation on Dissolution Kinetics of Glass Fibers in Polymer Composites. *Journal of Composites Science* 2022, 6, 210, doi:10.3390/jcs6070210.
65. Blowes, D.W.; Ptacek, C.J.; Jambor, J.L.; Weisener, C.G.; Paktunc, D.; Gould, W.D.; Johnson, D.B. 11.5 - The Geochemistry of Acid Mine Drainage. In *Treatise on Geochemistry* (Second Edition); Holland, H.D., Turekian, K.K., Eds.; Elsevier: Oxford, 2014; pp. 131–190 ISBN 978-0-08-098300-4.
66. Sujatha, D.; Reddy, B.R. Quality Characterization of Groundwater in the South-Eastern Part of the Ranga Reddy District, Andhra Pradesh, India. *Env Geol* 2003, 44, 579–586, doi:10.1007/s00254-003-0794-1.
67. Selvam, S.; Venkatramanan, S.; Chung, S.Y.; Singaraja, C. Identification of Groundwater Contamination Sources in Dindugal District of Tamil Nadu, India Using GIS and Multivariate Statistical Analyses. *Arabian Journal of Geosciences* 2016, 5, 1–14, doi:10.1007/s12517-016-2417-7.
68. Mokadem, N.; Dennis, R.; Dennis, I. Hydrochemical and Stable Isotope Data of Water in Karst Aquifers during Normal Flow in South Africa. *Environ Earth Sci* 2021, 80, 519, doi:10.1007/s12665-021-09845-7.
69. Rishi, M.S.; Kaur, L.; Sharma, S. Groundwater Quality Appraisal for Non-Carcinogenic Human Health Risks and Irrigation Purposes in a Part of Yamuna Sub-Basin, India. *Human and Ecological Risk Assessment: An International Journal* 2020, 26, 2716–2736, doi:10.1080/10807039.2019.1682514.

70. Liu, G.; Zhang, Y.; Knibbe, W.-J.; Feng, C.; Liu, W.; Medema, G.; van der Meer, W. Potential Impacts of Changing Supply-Water Quality on Drinking Water Distribution: A Review. *Water Research* 2017, 116, 135–148, doi:10.1016/j.watres.2017.03.031.
71. Svensson, T.; Kylin, H.; Montelius, M.; Sandén, P.; Bastviken, D. Chlorine Cycling and the Fate of Cl in Terrestrial Environments. *Environ Sci Pollut Res* 2021, 28, 7691–7709, doi:10.1007/s11356-020-12144-6.
72. Mokadem, N.; Demdoun, A.; Hamed, Y.; Bouri, S.; Hadji, R.; Boyce, A.; Laouar, R.; Sâad, A. Hydrogeochemical and Stable Isotope Data of Groundwater of a Multi-Aquifer System: Northern Gafsa Basin – Central Tunisia. *Journal of African Earth Sciences* 2016, 114, 174–191, doi:10.1016/j.jafrearsci.2015.11.010.
73. Guerzou, M.; Aouissi, H.A.; Guerzou, A.; Burlakovs, J.; Doumandji, S.; Krauklis, A.E. From the Beehives: Identification and Comparison of Physicochemical Properties of Algerian Honey. *Resources* 2021, 10, 94, doi:10.3390/resources1010094.
74. Das, N.; Sarma, K.P.; Patel, A.K.; Deka, J.P.; Das, A.; Kumar, A.; Shea, P.J.; Kumar, M. Seasonal Disparity in the Co-Occurrence of Arsenic and Fluoride in the Aquifers of the Brahmaputra Flood Plains, Northeast India. *Environ Earth Sci* 2017, 76, 183, doi:10.1007/s12665-017-6488-x.
75. Jain, C.K.; Sharma, S.K.; Singh, S. Physico-Chemical Characteristics and Hydrogeological Mechanisms in Groundwater with Special Reference to Arsenic Contamination in Barpeta District, Assam (India). *Environ Monit Assess* 2018, 190, 417, doi:10.1007/s10661-018-6781-5.
76. A Graphic Procedure in the Geochemical Interpretation of Water-Analyses. *Eos, Transactions American Geophysical Union* 1944, 25, 914–928, doi:10.1029/TR025i006p00914.
77. Thilagavathi, R.; Chidambaram, S.; Prasanna, M.V.; Thivya, C.; Singaraja, C. A Study on Groundwater Geochemistry and Water Quality in Layered Aquifers System of Pondicherry Region, Southeast India. *Appl Water Sci* 2012, 2, 253–269, doi:10.1007/s13201-012-0045-2.
78. Pant, D.; Keesari, T.; Rishi, M.S.; Sharma, D.A.; Jaryal, A.; Kamble, S.N.; Sinha, U.K. Hydrochemical Evolution of Groundwater in the Waterlogged Area of Southwest Punjab. *Arab J Geosci* 2020, 13, 773, doi:10.1007/s12517-020-05795-9.
79. Stumm, W.; Morgan, J.J. *Aquatic Chemistry: Chemical Equilibria and Rates in Natural Waters*; Wiley, 1996; ISBN 978-0-471-51184-7.
80. Chadha, D.K. A Proposed New Diagram for Geochemical Classification of Natural Waters and Interpretation of Chemical Data. *Hydrogeology Journal* 1999, 7, 431–439, doi:10.1007/s100400050216.
81. Gibbs, R.J. Mechanisms Controlling World Water Chemistry. *Science* 1970, 170, 1088–1090, doi:10.1126/science.170.3962.1088.
82. Li, P.; Wu, J.; Qian, H. Preliminary Assessment of Hydraulic Connectivity between River Water and Shallow Groundwater and Estimation of Their Transfer Rate during Dry Season in the Shidi River, China. *Environ Earth Sci* 2016, 75, 99, doi:10.1007/s12665-015-4949-7.
83. Chebotarev, I.I. Metamorphism of Natural Waters in the Crust of Weathering—1. *Geochimica et Cosmochimica Acta* 1955, 8, 22–48, doi:10.1016/0016-7037(55)90015-6.
84. Fisher, R.S.; William F. Mullican, I.I.I. Hydrochemical Evolution of Sodium-Sulfate and Sodium-Chloride Groundwater Beneath the Northern Chihuahuan Desert, Trans-Pecos, Texas, USA. *Hydrogeology Journal* 1997, 2, 4–16.
85. *Geochemistry, Groundwater and Pollution*; Appelo, C.A.J., Appelo, C.A.J., Postma, D., Postma, D., Eds.; 2nd ed.; CRC Press: London, 2005; ISBN 978-0-429-15232-0.

86. Kumari, R.; Datta, P.S.; Rao, M.S.; Mukherjee, S.; Azad, C. Anthropogenic Perturbations Induced Groundwater Vulnerability to Pollution in the Industrial Faridabad District, Haryana, India. *Environ Earth Sci* 2018, 77, 187, doi:10.1007/s12665-018-7368-8.
87. Hardie, L.W.A.; Eugster, H.P. THE EVOLUTION OF CLOSED-BASIN BRINES. 18.
88. Xiao, J.; Jin, Z.D.; Wang, J.; Zhang, F. Hydrochemical Characteristics, Controlling Factors and Solute Sources of Groundwater within the Tarim River Basin in the Extreme Arid Region, NW Tibetan Plateau. *Quaternary International* 2015, 380–381, 237–246, doi:10.1016/j.quaint.2015.01.021.
89. Zhu, B.; Yang, X.; Rioual, P.; Qin, X.; Liu, Z.; Xiong, H.; Yu, J. Hydrogeochemistry of Three Watersheds (the Erlqis, Zhungar and Yili) in Northern Xinjiang, NW China. *Applied Geochemistry* 2011, 26, 1535–1548, doi:10.1016/j.apgeochem.2011.06.018.
90. Gaillardet, J.; Dupré, B.; Louvat, P.; Allègre, C.J. Global Silicate Weathering and CO₂ Consumption Rates Deduced from the Chemistry of Large Rivers. *Chemical Geology* 1999, 159, 3–30, doi:10.1016/S0009-2541(99)00031-5.
91. Yang, Q.; Li, Z.; Ma, H.; Wang, L.; Martín, J.D. Identification of the Hydrogeochemical Processes and Assessment of Groundwater Quality Using Classic Integrated Geochemical Methods in the Southeastern Part of Ordos Basin, China. *Environmental Pollution* 2016, 218, 879–888, doi:10.1016/j.envpol.2016.08.017.
92. Mohammad, A.H.; Abdullat, G.; Alzughoul, K. Changes in Total Dissolved Solids Concentration during Infiltration through Soils (Rain, Fresh Groundwater and Treated Wastewater). *Journal of Environmental Protection* 2017, 8, 34–41, doi:10.4236/jep.2017.81004.
93. He, Z.; Ding, Q.; Wo, Y.; Zhang, J.; Fan, M.; Yue, X. Experiment of Carbonate Dissolution: Implication for High Quality Carbonate Reservoir Formation in Deep and Ultradeep Basins. *Geofluids* 2017, 2017, e8439259, doi:10.1155/2017/8439259.
94. Praus, P. Evaluation of Biological Wastewater Treatment Process Using Mahalanobis Distances in Original and Principal Component Space: A Case Study. *Appl Water Sci* 2018, 8, 167, doi:10.1007/s13201-018-0794-7.
95. Srivastava, S.K.; Ramanathan, A.L. Geochemical Assessment of Groundwater Quality in Vicinity of Bhalswa Land-fill, Delhi, India, Using Graphical and Multivariate Statistical Methods. *Environ Geol* 2008, 53, 1509–1528, doi:10.1007/s00254-007-0762-2.
96. Kraiem, Z.; Zouari, K.; Chkir, N.; Agoune, A. Geochemical Characteristics of Arid Shallow Aquifers in Chott Djerid, South-Western Tunisia. *Journal of Hydro-environment Research* 2014, 8, 460–473, doi:10.1016/j.jher.2013.06.002.
97. Byrne, M.P.; Tobin, J.T.; Forrestal, P.J.; Danaher, M.; Nkwonta, C.G.; Richards, K.; Cummins, E.; Hogan, S.A.; O'Callaghan, T.F. Urease and Nitrification Inhibitors—As Mitigation Tools for Greenhouse Gas Emissions in Sustainable Dairy Systems: A Review. *Sustainability* 2020, 12, 6018, doi:10.3390/su12156018.
98. Dalton, M.G.; Upchurch, S.B. Interpretation of Hydrochemical Facies by Factor Analysis. *Groundwater* 1978, 16, 228–233, doi:10.1111/j.1745-6584.1978.tb03229.x.
99. Güler, C.; Thyne, G.D.; McCray, J.E.; Turner, K.A. Evaluation of Graphical and Multivariate Statistical Methods for Classification of Water Chemistry Data. *Hydrogeology Journal* 2002, 10, 455–474, doi:10.1007/s10040-002-0196-6.
100. Halecki, W.; Stachura, T.; Fudała, W.; Rusnak, M. Evaluating the Applicability of MESS (Matrix Exponential Spatial Specification) Model to Assess Water Quality Using GIS Technique in Agricultural Mountain Catchment (Western Carpathian). *Environ Monit Assess* 2018, 191, 26, doi:10.1007/s10661-018-7137-x.
101. Aflatooni, M. Time Series Analysis of Ground Water Table Fluctuations Due to Temperature and Rainfall Change in Shiraz Plain.

-
102. Alam, S.; Khan, M.S.; Bibi, W.; Zekker, I.; Burlakovs, J.; Ghangrekar, M.M.; Bhowmick, G.D.; Kallistova, A.; Pimenov, N.; Zahoor, M. Preparation of Activated Carbon from the Wood of Paulownia Tomentosa as an Efficient Adsorbent for the Removal of Acid Red 4 and Methylene Blue Present in Wastewater. *Water* 2021, 13, 1453, doi:10.3390/w13111453.
 103. Alam, S.; Ullah, B.; Khan, M.S.; Rahman, N. ur; Khan, L.; Shah, L.A.; Zekker, I.; Burlakovs, J.; Kallistova, A.; Pimenov, N.; et al. Adsorption Kinetics and Isotherm Study of Basic Red 5 on Synthesized Silica Monolith Particles. *Water* 2021, 13, 2803, doi:10.3390/w13202803.
 104. Wahsner, J.; Gale, E.M.; Rodríguez-Rodríguez, A.; Caravan, P. Chemistry of MRI Contrast Agents: Current Challenges and New Frontiers. *Chem Rev* 2019, 119, 957–1057, doi:10.1021/acs.chemrev.8b00363.
 105. Taussi, M.; Gozzi, C.; Vaselli, O.; Cabassi, J.; Menichini, M.; Doveri, M.; Romei, M.; Ferretti, A.; Gambioli, A.; Nisi, B. Contamination Assessment and Temporal Evolution of Nitrates in the Shallow Aquifer of the Metauro River Plain (Adriatic Sea, Italy) after Remediation Actions. *International Journal of Environmental Research and Public Health* 2022, 19, 12231, doi:10.3390/ijerph191912231.